Research Square

Preprints are preliminary reports that have not undergone peer review.
They should not be considered conclusive, used to inform clinical practice,
or referenced by the media as validated information.

Limit laws for shallow loops in planar Gaussian kernel density estimates

Jiaxuan Ren

jiaxuanren@ucsb.edu

University of California, Santa Barbara

Research Article

Keywords: Persistent homology, kernel density estimation, topological data analysis, local asymptotics, limit distributions, angular moment designs

Posted Date: November 13th, 2026

DOI: https://doi.org/10.21203/rs.3.rs-11708798/v1

License: This work is licensed under a Creative Commons Attribution 4.0 International License.
Read Full License

Additional Declarations: No competing interests reported.

Limit laws for shallow loops in planar Gaussian kernel density estimates

Jiaxuan Ren[1*]

[1*]University of California, Santa Barbara, California, USA.

Corresponding author(s). E-mail(s): jiaxuanren@ucsb.edu;

Abstract

A shallow hole in a smoothed density may disappear when the density is estimated from a finite sample. I study this transition through the longest finite bar in the degree-one persistent homology of the closed superlevel sets of a planar Gaussian kernel density estimator with fixed bandwidth. For a Gaussian-difference density family and a circular family with Gaussian observation error, local parameter displacements of order $n^{-1/3}$ produce bar lengths of order $n^{-2/3}$. The rescaled longest bar converges to an explicit law determined by a quartic potential with a Gaussian linear tilt. For a fixed positive local parameter s, the law has an atom at zero, and the probability of a positive bar converges to $1-\exp(-\kappa_{\mathrm{occ}} s^3)$, with an explicit model-dependent constant $\kappa_{\mathrm{occ}} > 0$; this probability tends to zero for $s \leq 0$. The proof identifies the saddle–minimum persistence pairing and reduces the full-plane persistence module to a fixed disk with probability tending to one. Within the circular family, central symmetry and agreement with the uniform circle's polynomial moments through degree four yield a common first-order law, covering both discrete and continuous angular arrangements. Numerical studies examine finite-sample curvature effects and compare uniform-circle, regular-hexagon, and regular-octagon samples.

Keywords: Persistent homology, kernel density estimation, topological data analysis, local asymptotics, limit distributions, angular moment designs

MSC Classification: 62G07 , 62G20 , 55N31 , 60F05

Introduction

A hole in a density superlevel set can be present in the population and absent from its empirical estimate. This is especially likely near a transition at which the hole first

opens: the surrounding ridge is shallow, so a small spatial perturbation can remove the enclosed component. Persistent homology measures the range of density levels over which the hole survives. The question studied here is how the length and the very existence of this persistence bar behave when the population approaches the transition as the sample size increases.

This question is motivated in part by ring-shaped structures in localization microscopy. Pike et al. (2020) use persistent homology of point clouds to quantify holes in nuclear-pore protein clusters. The present paper studies a simplified statistical counterpart: closed superlevel sets of a planar Gaussian kernel density estimator (KDE) at a fixed smoothing scale. Its object is the longest finite degree-one persistence bar of the continuous estimator on the whole plane. The distinction between an underlying structure and a hole visible after smoothing and sampling is central to this formulation.

I consider two sampling settings: an explicit Gaussian-difference density family and a circular family with fixed Gaussian observation error. At their critical parameter, the quadratic term of the population smoother vanishes at the origin, while the leading radial spatial term is quartic. The resulting local geometry differs from the Morse setting in which critical points are nondegenerate. On the positive side of the transition, a small random tilt can leave a saddle–minimum pair, or merge the pair and erase the hole. Figures 1–2 display this pairing and the associated limiting occurrence probability.

Main results and contributions.

Here is the common form of the result, with the precise model assumptions and constants given in Theorems 2.1 and 6.1. Move the model parameter a distance $sn^{-1/3}$ from its critical value, with s fixed, and let L_n be the longest finite positive H_1 bar length, set equal to zero when no such bar exists. For positive model-dependent constants a, b, σ, the limiting field is

$$Q_{s,g}(u) = as|u|^2 - b|u|^4 + g \cdot u, \qquad G \sim N(0, \sigma^2 I_2).$$

Writing $\Psi_s(g)$ for the persistence length of this field, the two conclusions are

$$n^{2/3} L_n \Rightarrow \Psi_s(G), \qquad \Pr(L_n > 0) \longrightarrow \begin{cases} 1 - \exp(-\kappa_{\mathrm{occ}} s^3), & s > 0, \\ 0, & s \le 0, \end{cases} \qquad \kappa_{\mathrm{occ}} = \frac{4a^3}{27 b \sigma^2}.$$

For $s > 0$, the limiting length has a positive atom at zero. Thus a hole in the smoothed population can remain undetected with nonvanishing probability throughout this local parameter window. The positive part of the length distribution is explicit through the saddle and minimum of a cubic critical-point equation. The occurrence statement is proved by comparing events; convergence of lengths alone would not determine the mass at zero.

The scales follow from a simple balance. After subtracting the estimator's value at the origin, its leading stochastic term is the empirical gradient, of size $n^{-1/2}$, multiplied by the spatial displacement. A quartic population profile balances this linear tilt at radius $n^{-1/6}$. At that radius, a parameter displacement of order $n^{-1/3}$ and the random tilt both affect heights at order $n^{-2/3}$. The remaining task is to show that this local

field describes a persistence bar of the original estimator. A critical-height difference must have the correct persistence pairing, and features outside the local region must be controlled before the longest bar on the whole plane can be identified.

The paper makes three contributions.

1. It gives a critical-window limit law for the longest finite bar, including its zero atom and a separate limit for the positive-bar event. A representation using the gradient from the same sample connects the asymptotic law to observable empirical fluctuations.
2. It identifies the closed-superlevel persistence module of the quartic field and transfers the pairing to the continuous estimator. Exterior estimates provide a natural isomorphism between the full-plane module and a fixed-disk module with probability tending to one.
3. It shows that a common first-order law holds across a circular moment-design class. Central symmetry and agreement with the uniform circle's polynomial moments through degree four suffice; full rotational symmetry is unnecessary. The class includes the uniform circle, regular even polygons with at least six vertices, and mixtures of their rotations, with parameters and angular law fixed.

Related work.

The relation to existing topological inference is through both the filtration and the inferential question. Persistence-diagram stability controls bottleneck distance by uniform function error on a suitable common domain (Cohen-Steiner et al. 2007). Bobrowski, Mukherjee and Taylor (2017) recover superlevel-set homology through the image of inclusion-induced maps between kernel-selected unions of balls, using compactly supported kernels and shrinking bandwidths. Fasy et al. (2014, §4.4) construct confidence sets for diagrams of smoothed densities, including fixed bandwidth. Phillips, Wang and Zheng (2015) connect Gaussian kernel density superlevel sets to kernel-distance sublevel sets and obtain reconstruction and approximation results. Carlsson and Carlsson (2026) construct homotopy-equivalent geometric models of Gaussian kernel density superlevel sets and use finite alpha complexes for density-filtered persistence calculations. These results explain how density-based topology can be recovered, approximated, or assigned uncertainty. Here the target is the limiting lifetime and occurrence of a bar at a degeneracy where that bar is being created.

Probabilistic limits for persistence also depend on the geometric regime. Chazal et al. (2018, Lemmas 17–18 and Theorem 19) obtain a $\sqrt{n}$-scaled bottleneck-distance limit through Morse critical-point continuation and separation of critical values. Thomas (2025) proves strong laws and central limit theorems for functionals of zero-dimensional persistence diagrams of stationary scalar processes, under specified dependence and moment conditions. The present problem instead concerns a two-dimensional estimator in a shrinking neighborhood of a quartically degenerate transition. Its longest bar lives on a different scale, and its disappearance must be resolved through the local geometry and the global filtration.

The balance between a higher-order population term and a random linear perturbation has precedents in nonstandard limit theory. Eltzner and Huckemann (2019) study

higher-order expansions for empirical extrema, and Tran (2021) treats a radial fourth-order Fréchet-mean setting. Hall and Ooi (2004) analyze shape-event probabilities for a one-dimensional shrinking-bandwidth density estimator. Chen and Fang (2019) develop second-order inference when the first-order derivative vanishes. In this paper the additional geometric work identifies the relevant ordinary persistence bar, controls its exterior competitors, and establishes the separate limit for its occurrence probability.

The finite-sample studies illustrate the same mechanism in both sampling settings. In the Gaussian-difference model, comparisons use the gradient and full empirical Hessian from each sample to examine curvature effects beyond the leading tilt approximation. In the circular family, empirical curves from uniform-circle, regular-hexagon, and regular-octagon samples are compared with their common limiting law. Each experiment retains its specified numerical statistic and error budget; their finite-sample discrepancies are part of the reported results.

Sections 1–2 give the first model and its main theorem. Sections 3–5 establish the full-plane reduction and proof. Section 6 treats angular moment designs, Section 7 presents the numerical studies, and Section 8 discusses statistical interpretation and further directions. Appendices A–C contain the probability estimates, shared deterministic topology, and circular-design proof. Additional localization and equivariance results are provided in Online Resource 1.

1 Model and conventions

The first model subtracts a narrower Gaussian component from a Gaussian density. Its explicit population smoother permits direct calculation of the transition parameter and limit-law constants.

For $v > 0$ let

$$\phi_v(x) = (2\pi v)^{-1} \exp\{-|x|^2/(2v)\}, \qquad x \in \mathbb{R}^2.$$

The subscript denotes variance. Fix q in $(0, 1)$ and a kernel variance $H > 0$ satisfying $H^2 < q$. Write

$$v_1 = 1 + H, \quad v_2 = q + H, \quad e = \frac{v_2^2}{q v_1^2}, \quad D_c = 1 - eq.$$

At parameter e, the quadratic term of the population smoother vanishes at the origin. Then $0 < e < 1$. For $0 < \varepsilon < 1$ define the probability density

$$f_\varepsilon(x) = \frac{\phi_1(x) - \varepsilon q \phi_q(x)}{1 - \varepsilon q}.$$

Indeed $q\phi_q \le \phi_1$, and the numerator integrates to $1 - \varepsilon q$. Fix s in $\mathbb{R}$ and set $\varepsilon_n = e + sn^{-1/3}$. For all sufficiently large n this is an admissible parameter. The finitely many earlier rows may be omitted or assigned any admissible row distributions with the same KDE definition; this has no effect on the asymptotic assertions. In row

n, observations $X_{n1}, \dots, X_{nn}$ are independent and identically distributed (iid) with density f_{ε_n}; independence between rows is unnecessary. Define

$$\widehat{f}_n(x) = \frac{1}{n} \sum_{i=1}^{n} \phi_H(x - X_{ni}).$$

Throughout, the estimator is continuous and defined on the whole plane. Fix a coefficient field k. At filtration parameter z I take ordinary singular homology $H_1(\{\widehat{f}_n \geq -z\}; k)$, with maps induced by inclusion as z increases. Let L_n be its longest finite positive bar length, taking value zero when there is no such bar. Section 3 establishes that this statistic is defined for every finite sample and is Borel measurable.

The population smoother is $m_\varepsilon(x) = p_\varepsilon(|x|^2)$, where

$$A_0 = (2\pi v_1)^{-1}, \quad B = \frac{q}{2\pi v_2}, \qquad p_\varepsilon(w) = \frac{A_0 e^{-w/(2v_1)} - \varepsilon B e^{-w/(2v_2)}}{1 - \varepsilon q}.$$

Three constants determine the local limit: a describes the change of the quadratic term with the model parameter, b is the magnitude of the negative quartic coefficient, and σ_g^2 is the variance of each coordinate of the limiting empirical gradient. They are

$$a = \frac{B}{2v_2 D_c}, \qquad b = \frac{A_0(v_1/v_2 - 1)}{8 v_1^2 D_c} > 0,$$

$$\sigma_g^2 = \frac{(H+2)^{-2} - e q^2 (H+2q)^{-2}}{4\pi^2 H^2 D_c} > 0.$$

Here H denotes only kernel variance; H_1 denotes homology. Probability error tolerances will be denoted δ.

The recentered, rescaled field and its gradient at the origin are

$$G_n = \sqrt{n} \nabla \widehat{f}_n(0), \qquad F_n(u) = n^{2/3} \{\widehat{f}_n(n^{-1/6} u) - \widehat{f}_n(0)\}.$$

The common centering translates bar endpoints equally and leaves their difference unchanged.

2 Main theorem

Put $U = as$ and $Q_{s,g}(u) = U|u|^2 - b|u|^4 + g \cdot u$.

The three scales.

Write $d_n = \varepsilon_n - e$. The leading terms of $\widehat{f}_n(x) - \widehat{f}_n(0)$ near the origin are

$$a d_n |x|^2 - b|x|^4 + n^{-1/2} G_n \cdot x.$$

The gradient central limit theorem (CLT) in Appendix A.2 makes G_n of order one. Balancing the quartic term at radius r with the random tilt gives $r^4 \asymp n^{-1/2} r$, hence

$r \asymp n^{-1/6}$. Balancing the magnitude $|d_n|r^2$ with r^4 suggests the local parameter scale $n^{-1/3}$. The population terms and random tilt are therefore compared on the $n^{-2/3}$ height scale. Thus $x = n^{-1/6}u$ and $d_n = sn^{-1/3}$ produce Q_{s,G_n} after multiplying heights by $n^{2/3}$.

To obtain the limiting bar length, I use the critical points of the quartic field. Define $\Psi_s(g)$ as follows. For $U \le 0$ it is zero. For $U > 0$ put

$$t = |g|, \qquad t_c = \frac{4U^{3/2}}{3\sqrt{6b}}.$$

At $t = 0$, $\Psi_s(g) = U^2/(4b)$; for $t \ge t_c$ it is zero. When $0 < t < t_c$, let $x_1 < x_2 < x_3$ be the roots of

$$2Ux - 4bx^3 + t = 0.$$

Set $S = 3bx_1^4 - Ux_1^2$ and $m = 3bx_2^4 - Ux_2^2$; then $\Psi_s(g) = S - m$. In this three-root regime, rotating the tilt onto the first coordinate places the saddle at $(x_1, 0)$ and the enclosed minimum at $(x_2, 0)$. Their heights are S and m, so $S - m$ is the lifetime illustrated in Figure 1; Theorem B.3 verifies the persistence pairing.

Theorem 2.1 *Fix the parameters above. Choose any fixed sufficiently small ρ in $(0, 1)$ such that $p_e'' \le -3b/2$ on $[0, \rho^2]$, and write $D_\rho = \{|x| \le \rho\}$. Let L_n^D denote the longest finite bar of the same estimator restricted to D_ρ. There exist Borel events Ω_n, with $\Pr(\Omega_n) \to 1$, on which inclusion of D_ρ into $\mathbb{R}^2$ induces a natural isomorphism of the complete H_1 persistence modules, and these modules have zero or one positive bar. For G distributed as $N(0, \sigma_g^2 I_2)$,*

$$\Pr(L_n = L_n^D) \longrightarrow 1, \qquad n^{2/3} L_n \Rightarrow \Psi_s(G).$$

Moreover,

$$\Pr(L_n > 0) \longrightarrow \begin{cases} 1 - \exp\{-t_c^2/(2\sigma_g^2)\}, & s > 0, \\ 0, & s \le 0. \end{cases}$$

Remark (Same-sample representation) Section 5 also proves

$$n^{2/3} L_n - \Psi_s(G_n) \xrightarrow{P} 0, \qquad (n^{2/3} L_n, G_n) \Rightarrow (\Psi_s(G), G).$$

Indeed, the first assertion is the comparison on Ω_n and its probability bound; continuity of $g \mapsto (\Psi_s(g), g)$, the gradient CLT, and Slutsky's theorem give the second. This representation supports paired comparisons using the gradient computed from the same sample.

Remark (The limiting module) Theorem B.3 identifies the closed-superlevel module of $Q_{s,g}$ as $k_{[-S,-m)}$ in the three-root regime, as $k_{[-U^2/(4b),0)}$ when $U > 0$ and $t = 0$, and as zero otherwise. Birth is included and death is excluded. At $t = t_c$ the saddle and minimum collide, and the module is zero at every filtration parameter. The same theorem proves continuity of Ψ_s at zero tilt and at the cusp.

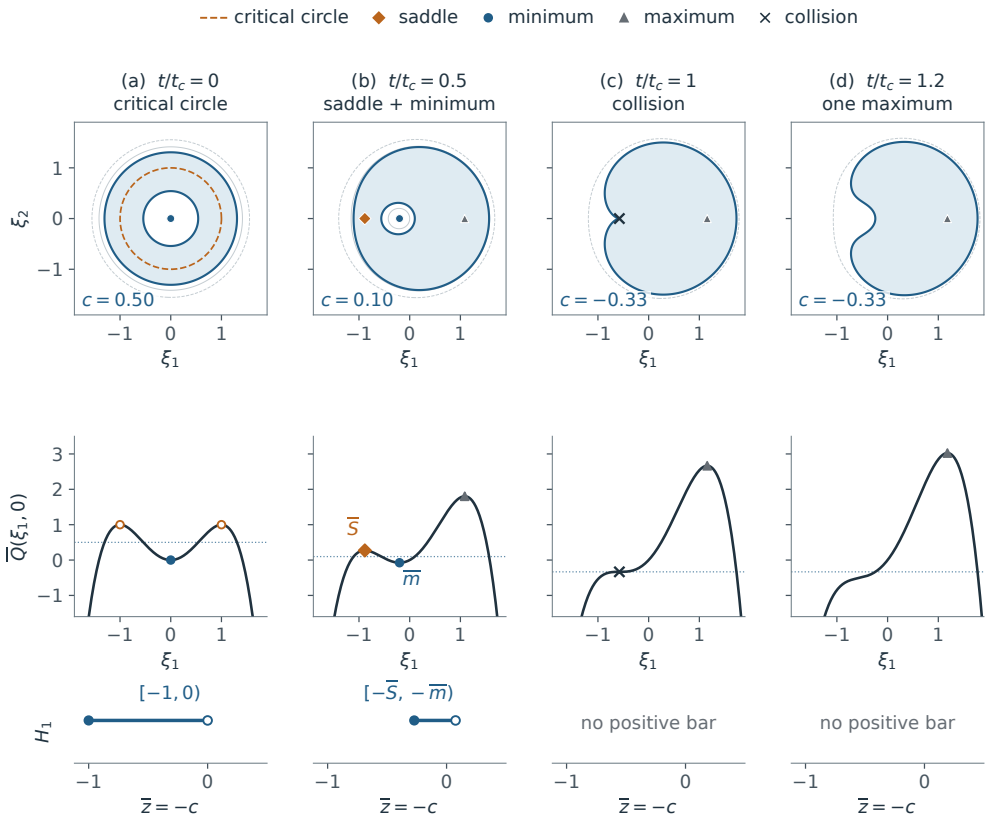


Fig. 1 The quartic transition under increasing tilt. For $U > 0$, rotate the tilt onto the first coordinate and put $r_0 = \sqrt{U/(2b)}$, $C_0 = U^2/(4b)$, and $\xi = u/r_0$. Then $\overline{Q}(\xi) = Q_{s,g}(r_0\xi)/C_0 = 2|\xi|^2 - |\xi|^4 + \frac{8}{3\sqrt{3}}\frac{t}{t_c}\xi_1$. The rows show shaded closed superlevels $\{\overline{Q} \geq c\}$, axial profiles, and the full H_1 bars with parameter $\overline{z} = -c$. The displayed height is $(\overline{S}+\overline{m})/2$ in (a)–(b) and $-1/3$ in (c)–(d), where $\overline{S} = S/C_0$, $\overline{m} = m/C_0$, and $(\overline{S}, \overline{m}) = (1, 0)$ at zero tilt. The critical circle in (a) yields $[-1, 0)$; the saddle and minimum in (b) yield $[-\overline{S}, -\overline{m})$. At the threshold they collide, leaving no positive bar; above it only the maximum remains. Filled and open endpoints denote included birth and excluded death.

Corollary 2.2 (Distribution of the limiting length) *Let $Y_s = \Psi_s(G)$. For $s > 0$, set $\ell_s = (as)^2/(4b)$ and $\psi_s(t) = \Psi_s((t, 0))$ for $t \geq 0$. The restriction of ψ_s to $[0, t_c]$ is continuous and strictly decreasing from ℓ_s to zero. Denote its inverse by $r_s : [0, \ell_s] \to [0, t_c]$, with $r_s(0) = t_c$ and $r_s(\ell_s) = 0$. Then*

$$\Pr(Y_s \leq y) = \begin{cases} 0, & y < 0, \\ \exp\{-r_s(y)^2/(2\sigma_g^2)\}, & 0 \leq y < \ell_s, \\ 1, & y \geq \ell_s. \end{cases}$$

In particular,

$$\Pr(Y_s = 0) = e^{-\kappa_{\mathrm{occ}} s^3}, \qquad \kappa_{\mathrm{occ}} = \frac{4a^3}{27b\sigma_g^2}.$$

There are no atoms in $(0, \ell_s]$. For $s \leq 0$, $Y_s = 0$ almost surely, so its cumulative distribution function (CDF) is $\mathbf{1}_{\{y \geq 0\}}$.

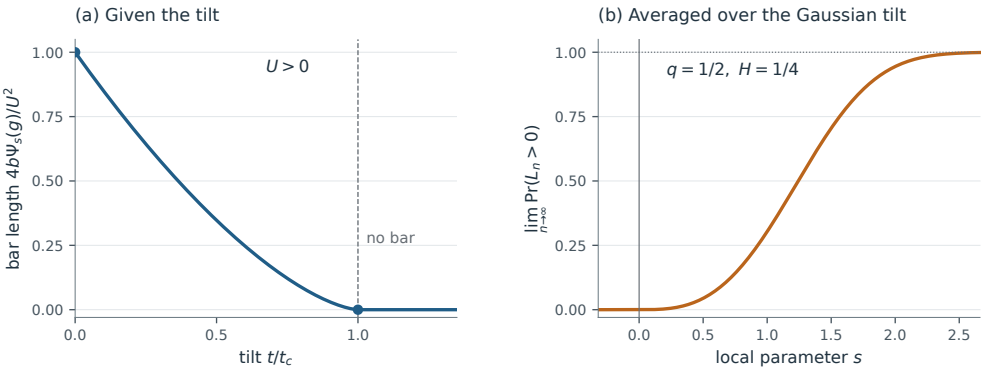


Fig. 2 Deterministic length and random existence. (a) The normalized length $4b\Psi_s(g)/U^2$ for $U > 0$, as a function of t/t_c. (b) The limiting probability from Theorem 2.1, as a function of the local parameter s, with $q = 1/2$ and kernel variance $H = 1/4$. Panel (a) fixes the tilt magnitude; panel (b) averages over $G \sim N(0, \sigma_g^2 I_2)$. Both panels evaluate the analytic formulas, without simulated samples.

Proof Theorem B.3 gives $\psi_s'(t) = x_1(t) - x_2(t) < 0$ on $(0, t_c)$ and the endpoint values. For $0 \le y < \ell_s$, $Y_s \le y$ is exactly $|G| \ge r_s(y)$. The Rayleigh tail proves the formula; substitution of t_c gives the zero mass. Strict monotonicity and $\Pr(|G| = 0) = 0$ exclude the remaining atoms. □

Finite-sample curvature.

The centered empirical Hessian contributes $O_P(n^{-5/6})$ to the original local height, or $O_P(n^{-1/6})$ after rescaling. Proposition A.2 bounds the full C^2 field error on each fixed disk. Retaining the complete quadratic coefficient $M_n = \frac{1}{2} n^{1/3} D^2 \widehat{f}_n(0)$ improves that local error bound to $O_P(n^{-1/3})$, as shown by Lemma A.3. This motivates comparing the tilt and full-Hessian approximations through paired absolute errors in Section 7. The matrix is generally anisotropic, and the local bound alone supplies no rate for bar lengths, their CDF, or exact occurrence probabilities.

Figures 1–2 illustrate the quartic pairing and its consequences for the limit law.

3 The statistic and the full-plane reduction

The reduction proceeds in two stages. For every finite sample, a sufficiently large disk captures the full-plane module and makes the statistic well defined. The exterior estimates then show that the same module is captured by the fixed small disk D_ρ with probability tending to one.

For each finite sample, choose $T > \max_i |X_i|$. Then

$$x \cdot \nabla \widehat{f}_n(x) = -\frac{1}{nH} \sum_i x \cdot (x - X_i) \phi_H(x - X_i) < 0, \qquad |x| \ge T.$$

The inward radial homotopy of Lemma B.2 never decreases the estimator and has the same formula at every level. It gives a natural isomorphism between the plane and disk persistence modules at every filtration parameter.

On the compact disk, the finite Gaussian sum is restricted-analytic definable. Proposition B.6 uses a single function-preserving triangulation to obtain a finite interval decomposition with closed births and open deaths. Every bar is finite because the terminal disk has zero H_1. This defines L_n on the sample space.

For samples X, Y of size n, the kernel gradient bound and Lemma B.5 give

$$|L(X) - L(Y)| \le \frac{2C_K}{n} \sum_i |X_i - Y_i|, \qquad C_K = \frac{e^{-1/2}}{2\pi H^{3/2}}.$$

Thus L_n and its positive-length event are Borel measurable. Strict radial decrease outside a fixed D_ρ gives the same natural reduction to that disk. I next establish this condition with probability tending to one.

4 Exterior control

Lemma 4.1 *For every fixed $\rho > 0$, the Borel event*

$$\mathcal{E}_n(\rho) = \{x \cdot \nabla \widehat{f}_n(x) < 0 \text{ for every } |x| \ge \rho\}$$

has probability tending to one.

The event is Borel by Proposition B.7. I prove radial decrease in two regions: concentration controls a growing annulus, and a bound on the sample radii handles its exterior.

Population signal.

Put $\Lambda = 1/(2v_2) - 1/(2v_1) > 0$. Direct differentiation gives

$$p'_\varepsilon(w) = -\frac{A_0 e^{-w/(2v_1)}}{2v_1(1-\varepsilon q)}[1 - (\varepsilon/e)e^{-\Lambda w}].$$

Let $\theta_0 = (1 + \exp(-\Lambda\rho^2))/2 < 1$. For large n the bracket is at least $1 - \theta_0$ on $w \ge \rho^2$. With $c_1 = (1-\theta_0)A_0/(2v_1)$ and $\tau(r) = c_1 r^2 \exp(-r^2/(2v_1))$,

$$x \cdot \nabla m_{\varepsilon_n}(x) \le -2\tau(|x|), \quad |x| \ge \rho.$$

Pointwise fluctuations.

Set $\xi_x(X) = x \cdot \nabla\phi_H(x - X)$, $r = |x|$. Its absolute value is at most $C_K r$, and its centered version is bounded by $M(r) = 2C_K r$. Since $f_\varepsilon \le \phi_1/(1-q)$ and $\phi_H^2 = (4\pi H)^{-1}\phi_{H/2}$, Gaussian completion of squares gives

$$\mathrm{Var}(\xi_x) \le V(r) = C_2 r^2(r^2+2)e^{-r^2/(2+H)}, \qquad C_2 = [H^2\, 4\pi H(1-q)\, 2\pi(1+H/2)]^{-1}.$$

Set $y = x - X$ in the second-moment integral. Since $\xi_x(X) = -H^{-1}(x \cdot y)\phi_H(y)$, the bound $(x \cdot y)^2 \le r^2|y|^2$ leaves the integral of $|y|^2\phi_{H/2}(y)\phi_1(x-y)$. Completing the square gives

$$\phi_{H/2}(y)\phi_1(x-y) = \phi_{1+H/2}(x)\phi_{w_0}(y - w_0 x), \qquad w_0 = \frac{H}{2+H}.$$

The normalized factor has mean $w_0 x$ and covariance $w_0 I_2$, so integration yields $w_0^2 r^2 + 2w_0 \le r^2 + 2$. Although this variance envelope decays faster than the signal amplitude, it decays more slowly than the squared signal. Accordingly,

$$\frac{\tau(r)^2}{V(r)} = \frac{c_1^2}{C_2}\frac{r^2}{r^2+2}\exp\left\{-\frac{r^2}{(1+H)(2+H)}\right\},$$

which is the comparison used in the growing-annulus estimate.

Bernstein's inequality, with conservative constants, gives

$$\Pr\left(\left|n^{-1}\sum_i(\xi_x(X_{ni}) - \mathbb{E}\xi_x)\right| \ge \tau(r)/2\right) \le 2\exp\left[-\min\left\{\frac{n\tau(r)^2}{16V(r)}, \frac{3n\tau(r)}{8M(r)}\right\}\right].$$

Growing annulus.

Choose $2 < \gamma < 2(1+H)$, put $R_n = \sqrt{\gamma \log n}$, and $\kappa = 1 - \gamma/[2(1+H)] > 0$. For $\rho \le r \le R_n$, the two exponents are bounded below, up to fixed positive constants, by

$$ne^{-r^2/[(1+H)(2+H)]}, \qquad nre^{-r^2/[2(1+H)]}.$$

Both are at least cn^κ. In the first bound the factor $r^2/(r^2+2)$ has a positive lower bound because $r \ge \rho$. Thus both the variance and envelope terms are controlled.

Let $Z_n = \widehat{f}_n - m_{\varepsilon_n}$ and $g_n(x) = x \cdot \nabla Z_n(x)$. Deterministically,

$$|\nabla g_n(x)| \le 2C_K + 2|x|C_{K,2}, \qquad C_{K,2} = \sup_x \|D^2\phi_H(x)\| < \infty.$$

An n^{-2}-net of the annulus has at most $C(\log n)n^4$ points. The probability of any net-point failure is bounded by $C(\log n)n^4\exp(-cn^\kappa)$. Also $\min\tau \ge cn^{-(1-\kappa)}$ for sufficiently large n, and $|(\log\tau)'| \le 2/\rho + R_n/v_1$. Consequently the net thresholds vary by a factor tending to one and the interpolation error $O((1+R_n)n^{-2})$ is $o(\min\tau)$. The net bounds extend to $|g_n| \le \tau$ over the whole closed annulus, yielding strict negativity of the empirical radial derivative there.

Outside the annulus.

The exact two-dimensional Gaussian radial tail and the density envelope imply

$$\Pr\{\max_i |X_{ni}| > R_n\} \le (1-q)^{-1}n^{1-\gamma/2} \longrightarrow 0.$$

On its complement, every kernel has strictly negative radial derivative for $|x| > R_n$. The boundary $|x| = R_n$ was already included in the closed annulus. Thus, for sufficiently large n,

$$\Pr(\mathcal{E}_n(\rho)^c) \le C(\log n)n^4 e^{-cn^\kappa} + (1-q)^{-1}n^{1-\gamma/2} \longrightarrow 0.$$

This proves the lemma. The constants and the starting n depend on the fixed parameters.

5 Proof of Theorem 2.1

Local approximation and localization. Use the recentered, rescaled field F_n and gradient G_n defined in Section 1, and the error $\Delta_{n,R}$ from Proposition A.2. The gradient CLT (A.7) gives $G_n \Rightarrow G \sim N(0, \sigma_g^2 I_2)$. For each fixed R, Proposition A.2 gives

$$\mathbb{E}\Delta_{n,R}^2 \le C_{s,R} n^{-1/3}.$$

For every sufficiently large fixed R, the inner-annulus event $E_{n,R}$ from (A.21) satisfies

$$\limsup_n \Pr(E_{n,R}^c) \le C/R^6$$

by (A.22). Lemma 4.1 controls the remaining physical exterior: $\Pr(\mathcal{E}_n(\rho)^c) \to 0$.

Persistence pairing. Theorem B.3 identifies the quartic model's complete module and its continuous length Ψ_s. On each nonempty compact set of tilts separated from zero and, when $s > 0$, the cusp circle, Theorem B.4 transfers the model's zero/one-bar classification and saddle–minimum pairing to nearby fields. Its tolerance is uniform over that compact set and is selected after the final inner radius. Proposition B.7 applies this result to F_n on the disk $D_{\rho n^{1/6}}$; the local approximation and full-annulus sign ensure the required boundary isolation.

Appendix A.6 combines these inputs by selecting deterministic $\Gamma_k, R_k, \eta_k, n_k$, in that order, with $\delta_k = 2^{-k}$ and $\eta_k \le \delta_k/2$. Its Borel events Ω_n in (A.27) satisfy $\Pr(\Omega_n^c) \to 0$, with $k(n) \to \infty$. On these events, Lemma B.2 identifies the complete plane and physical-disk modules naturally, and Proposition B.7 gives zero or one positive bar. In particular, $\Pr(L_n = L_n^D) \to 1$.

Length and occurrence limits. Spatial dilation and the common affine height change give, for every sample,

$$L(F_n; D_{\rho n^{1/6}}) = n^{2/3} L_n^D.$$

On Ω_n, the endpoint bounds in Proposition B.7 therefore yield

$$|n^{2/3}L_n - \Psi_s(G_n)| \le 2\Delta_{n,R_{k(n)}} < \delta_{k(n)}.$$

For every fixed $\epsilon > 0$, eventually $\delta_{k(n)} < \epsilon$, so

$$\Pr\{|n^{2/3}L_n - \Psi_s(G_n)| > \epsilon\} \le \Pr(\Omega_n^c) \longrightarrow 0.$$

Continuity of Ψ_s, the gradient CLT, and Slutsky's theorem prove the length limit. On the event $A_{n,k(n)}$ defined in (A.24), Proposition B.7 gives the same comparison and hence the same limit for L_n^D. The exterior reduction also gives

$$\Pr\{n^{2/3}|L_n - L_n^D| > \epsilon\} \le \Pr(\mathcal{E}_n(\rho)^c) \longrightarrow 0.$$

For the existence probability, let $B_s = \{g : 0 < |g| < t_c\}$ when $s > 0$, and $B_s = \varnothing$ otherwise. Proposition B.7 gives

$$\mathbf{1}_{\{L_n>0\}} = \mathbf{1}_{\{G_n \in B_s\}} \quad \text{on } \Omega_n, \qquad |\Pr(L_n > 0) - \Pr(G_n \in B_s)| \le \Pr(\Omega_n^c) \to 0.$$

When $s > 0$, the boundary of B_s has zero Gaussian measure, and (A.8) gives $\Pr(G \in B_s) = 1 - \exp\{-t_c^2/(2\sigma_g^2)\}$. For $s \le 0$, the exact zero-bar classification gives $\Pr(L_n > 0) \le \Pr(\Omega_n^c) \to 0$. The disk has the same existence limit: on $A_{n,k(n)}$ from (A.24), Proposition B.7 gives the disk indicator, and its probability error is bounded by $\Pr(A_{n,k(n)}^c) \to 0$. The fixed-disk conclusions follow on $A_{n,k(n)}$ from the same length and indicator bounds. This proves Theorem 2.1. □

6 Angular moment designs

Different angular arrangements can have the same critical persistence law because the local limit depends on only a few population coefficients and the covariance of the empirical gradient. Matching the circular moments through degree four fixes the quadratic and quartic terms. With isotropic Gaussian observation error, the second angular moment also fixes the gradient covariance. A separate exterior estimate then controls the complete plane module. This section treats a sampling family distinct from the Gaussian-difference family of Theorem 2.1.

Let ν be a fixed Borel probability measure on S^1, centrally symmetric in the sense that $\nu(A) = \nu(-A)$ for every Borel set A, and suppose

$$\int_{S^1} P(y)\, d\nu(y) = \frac{1}{2\pi} \int_0^{2\pi} P(\cos t, \sin t)\, dt \qquad (\deg P \le 4). \tag{6.1}$$

Here P ranges over real polynomials in two variables. I call this moment condition an angular probability 4-design; central symmetry is an additional assumption. The definition permits discrete, weighted, and continuous probability laws.

Fix the kernel variance $H > 0$, observation-error variance $\lambda \ge 0$, and $s \in \mathbb{R}$. Set $v = H + \lambda$, $e_{\mathrm{circ}} = 2v$, and $\theta_n = e_{\mathrm{circ}} + sn^{-1/3}$. For all sufficiently large n, take

$$X_{ni} = \sqrt{\theta_n} S_{ni} + \zeta_{ni}, \qquad S_{ni} \overset{\text{iid}}{\sim} \nu, \qquad \zeta_{ni} \overset{\text{iid}}{\sim} N(0, \lambda I_2), \tag{6.2}$$

with all variables independent within a row. At $\lambda = 0$ the errors vanish. The parameter θ is the squared circle radius; H and λ are variances. No independence between rows is required.

Write

$$\widehat{f}_n^{\circ}(x) = \frac{1}{n}\sum_{i=1}^{n} \phi_H(x - X_{ni}), \qquad \phi_H(x) = \frac{1}{2\pi H}\exp\{-|x|^2/(2H)\}.$$

For the uniform-circle law, the spatial density profile of the population smoother is $m_\theta(r) = p_{2,\theta/v}(r^2/v)/(\pi v)$, where $p_{2,\delta}$ is the noncentral χ^2 density with two degrees of freedom and noncentrality δ. Its transition at $\theta = 2v$, from a maximum at the origin to a maximum on a positive-radius circle, follows from the known mode classification (Yu 2011, Theorem 1 and Corollary 1).

Let L_n° be the longest positive finite H_1 bar of the continuous, full-plane filtration $z \mapsto \{\widehat{f}_n^{\circ} \geq -z\}$, taking zero when no positive bar exists, over any fixed coefficient field. Set $G_n^{\circ} = \sqrt{n}\nabla\widehat{f}_n^{\circ}(0)$. The circle-model constants are

$$C_{\mathrm{circ}} = \frac{\exp(-1)}{2\pi v}, \qquad a_{\mathrm{circ}} = \frac{C_{\mathrm{circ}}}{4v^2}, \qquad b_{\mathrm{circ}} = \frac{C_{\mathrm{circ}}}{16v^2}, \qquad d = 1 + \frac{2\lambda}{H}, \tag{6.3}$$

$$\sigma_{\mathrm{circ}}^2 = \frac{\exp\{-e_{\mathrm{circ}}/(Hd)\}}{8\pi^2 H^4}\left(\frac{2\lambda}{d^2} + \frac{e_{\mathrm{circ}}}{d^3}\right) > 0. \tag{6.4}$$

Define $Q_{s,g}^{\circ}(u) = a_{\mathrm{circ}} s|u|^2 - b_{\mathrm{circ}}|u|^4 + g\cdot u$ and let $\Psi_s^{\circ}(g)$ be its persistence length from Theorem B.3, with $U = a_{\mathrm{circ}} s$ and $b = b_{\mathrm{circ}}$. This includes the zero-tilt and collision endpoints.

Theorem 6.1 (Common circular-design limit) *Under these fixed-parameter assumptions, if $G^{\circ} \sim N(0, \sigma_{\mathrm{circ}}^2 I_2)$, then*

$$\begin{aligned} n^{2/3}L_n^{\circ} - \Psi_s^{\circ}(G_n^{\circ}) &\longrightarrow_P 0, \\ (n^{2/3}L_n^{\circ}, G_n^{\circ}) &\Rightarrow (\Psi_s^{\circ}(G^{\circ}), G^{\circ}). \end{aligned} \tag{6.5}$$

Moreover,

$$\begin{aligned} \Pr(L_n^{\circ} > 0) &\longrightarrow \begin{cases} 1 - \exp\{-(t_{\mathrm{circ}}(s))^2/(2\sigma_{\mathrm{circ}}^2)\}, & s > 0, \\ 0, & s \leq 0, \end{cases} \\ t_{\mathrm{circ}}(s) &= \frac{4(a_{\mathrm{circ}}s)^{3/2}}{3\sqrt{6b_{\mathrm{circ}}}} \quad (s > 0). \end{aligned} \tag{6.6}$$

For a sufficiently small physical disk D_ρ selected before sampling, there are Borel events of probability tending to one on which inclusion induces a natural isomorphism between its complete persistence module and the plane module. On these events the module has zero or one positive bar.

Two representative examples are the uniform circle and any mixture of rotations of uniform regular even polygons with at least six vertices. For a regular k-gon, the angular Fourier averages of orders $1, \ldots, 4$ vanish when $k \geq 5$; even k also supplies central symmetry. Both properties are preserved by rotation and mixing. Further examples and the role of the fourth moment appear in Appendix C.6.

Proof outline Appendix C derives the coefficients and weighted gradient covariance, then proves a fixed-compact C^2 approximation. Central symmetry and the circular moments give strict population decrease along every exterior ray at criticality. Compact-support or Gaussian-envelope estimates transfer this sign to the empirical exterior, and an inner-annulus bound connects it to the local field. The deterministic results of Appendix B, applied on measurable events, give the length comparison and a separate exact existence-indicator identity. □

The constants and limiting law are independent of ν for fixed H, λ, s. The result is pointwise in these parameters and the fixed angular law; finite-sample equality and uniform calibration are separate questions. Applications involving labeling, repeated localizations, or dependent nuclear-pore observations require an appropriate observation model.

7 Finite-sample behavior

The limit law describes a competition between a shallow population crater and a random tilt. At finite sample sizes, the same data also perturb the curvature. I first compare the numerical distribution with the limit law, then examine whether retaining empirical curvature improves the approximation for the same observations. The circular-family experiment compares three angular arrangements with a common limiting law.

Numerical scope.

The reported bars belong to finite-resolution numerical fields. A numerical zero means that no bar is resolved under the convention stated for that experiment; it does not certify absence of a bar of the continuous KDE. The Gaussian-difference budgets provide an empirical sensitivity analysis, whereas the circular-family bounds cover interpolation of the finite Fourier field. The reported binomial intervals describe numerical indicators.

Design and numerical resolution.

I use the Gaussian-difference model with $q = 1/2$, $H = 1/4$, and hence $e = 0.72$. For each $n \in \{10^4, 10^5\}$ and $s \in \{-1, 0, 1, 2\}$, I generate 400 independent samples at $\varepsilon_n = e + sn^{-1/3}$, giving 3,200 samples. The design, thresholds, numerical settings, and comparison rules were fixed before this run. All samples produced a numerical value.

Write $Y_n^{\mathrm{num}} = n^{2/3} L_n^{\mathrm{num}}$ for the computed statistic. The implementation uses a piecewise-linear (PL) field on a six-neighbour triangulation with grid spacing $0.08n^{-1/6}$, a virtual exterior component at the window boundary, and removal of bars no longer than the declared numerical noise floor. Thus $Y_n^{\mathrm{num}} = 0$ means absence of a resolved numerical bar. Each sample is accompanied by an empirical error budget for interpolation, field evaluation, and the removal of short bars. The median rescaled budgets range from 0.0044 to 0.0051 at $n = 10^4$ and from 0.0088 to 0.0095 at $n = 10^5$.

The main threshold is 0.05. The additional thresholds 0.005, 0.01, 0.02, 0.1, and 0.2 are retained in the numerical tables; the smallest two require particular caution relative to the budgets. The reported intervals use the Clopper–Pearson construction.

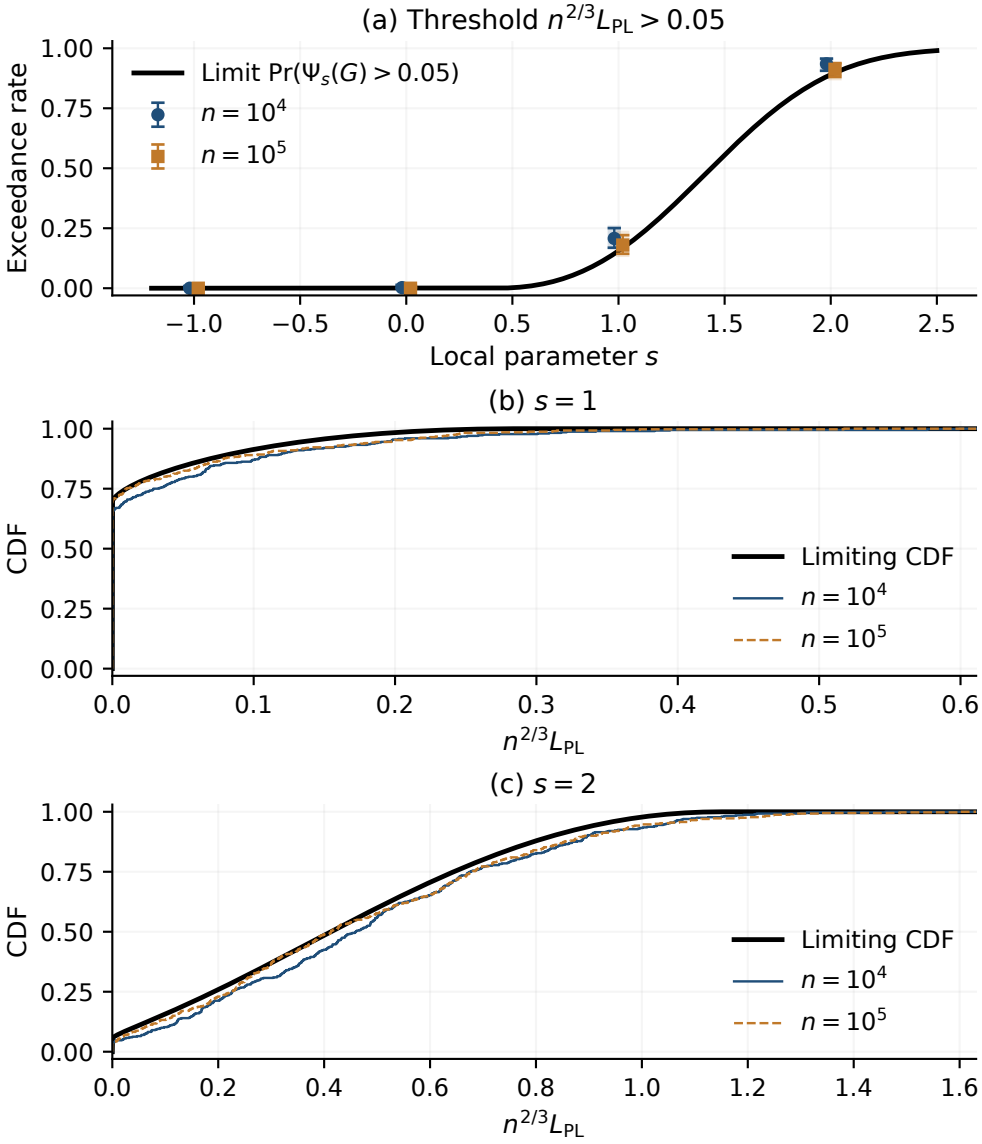


Fig. 3 Numerical threshold probabilities and distributions for the Gaussian-difference model. Panel (a) shows the numerical exceedance proportions at the preselected threshold 0.05, with nominal 95% binomial intervals and empirical-budget sensitivity envelopes. Panels (b)–(c) show numerical empirical CDFs for $s = 1, 2$ and the limiting CDF. Each empirical curve uses 400 samples. The jump at zero records samples with no grid bar above the declared noise floor. In Figures 3 and 4, the label $n^{2/3}L_{\mathrm{PL}}$ denotes Y_n^{num}.

Table 1 Mean absolute errors (MAEs) relative to Y_n^{num}, using all 400 paired samples in each cell. The ratio is full-Hessian MAE divided by tilt MAE. Values are rounded from the saved analysis.

n	s	Tilt MAE	Full-Hessian MAE	Ratio
10^4	1	0.0393	0.0161	0.41
10^4	2	0.267	0.147	0.55
10^5	1	0.0247	0.00682	0.28
10^5	2	0.202	0.0756	0.37

Comparison with the limiting distribution.

Figure 3 compares the numerical distribution with the explicit law of $\Psi_s(G)$.

At threshold 0.05, the limiting exceedance probabilities for $s = 1, 2$ are approximately 0.1555 and 0.8903. The observed proportions are 0.2075 and 0.9350 at $n = 10^4$, and 0.1800 and 0.9125 at $n = 10^5$. Both positive-s proportions move towards their limits as the sample size increases, while finite-sample differences remain. In particular, at $n = 10^5, s = 1$, the exceedance proportion at threshold 0.2 is $19/400 = 0.0475$, compared with a limit of approximately 0.0160.

A comparison using the same observations.

The marginal distribution does not reveal which fluctuation accounts for the error on a particular sample. For this purpose I compare Y_n^{num} with $\Psi_s(G_n)$ and with the persistence length of

$$\widetilde{Q}_n(u) = G_n \cdot u + u^\top M_n u - b|u|^4, \qquad M_n = \tfrac{1}{2} n^{1/3} D^2 \widehat{f}_n(0).$$

Both G_n and the full matrix M_n are evaluated from the same sample as the numerical statistic. Lemma A.3 motivates this comparison: retaining the empirical Hessian improves the approximation of the field on fixed compact sets. The Hessian's anisotropic part records directional curvature that its trace alone cannot distinguish.

In all four positive-s cells, the full-Hessian approximation has a smaller mean absolute error, with ratios between 0.28 and 0.55 (Table 1). Figure 4 displays the samplewise comparison. A preselected trace-only approximation has larger mean absolute errors than the full-matrix approximation in these cells. The improvement is not universal: at $s = 0, n = 10^5$, the full-Hessian MAE is approximately twice the tilt MAE, although both are below 1.2×10^{-6} and far below the numerical budget. Moreover, at $s = 2$ the full-Hessian residual errors remain appreciable: their MAEs are approximately 0.147 and 0.0756.

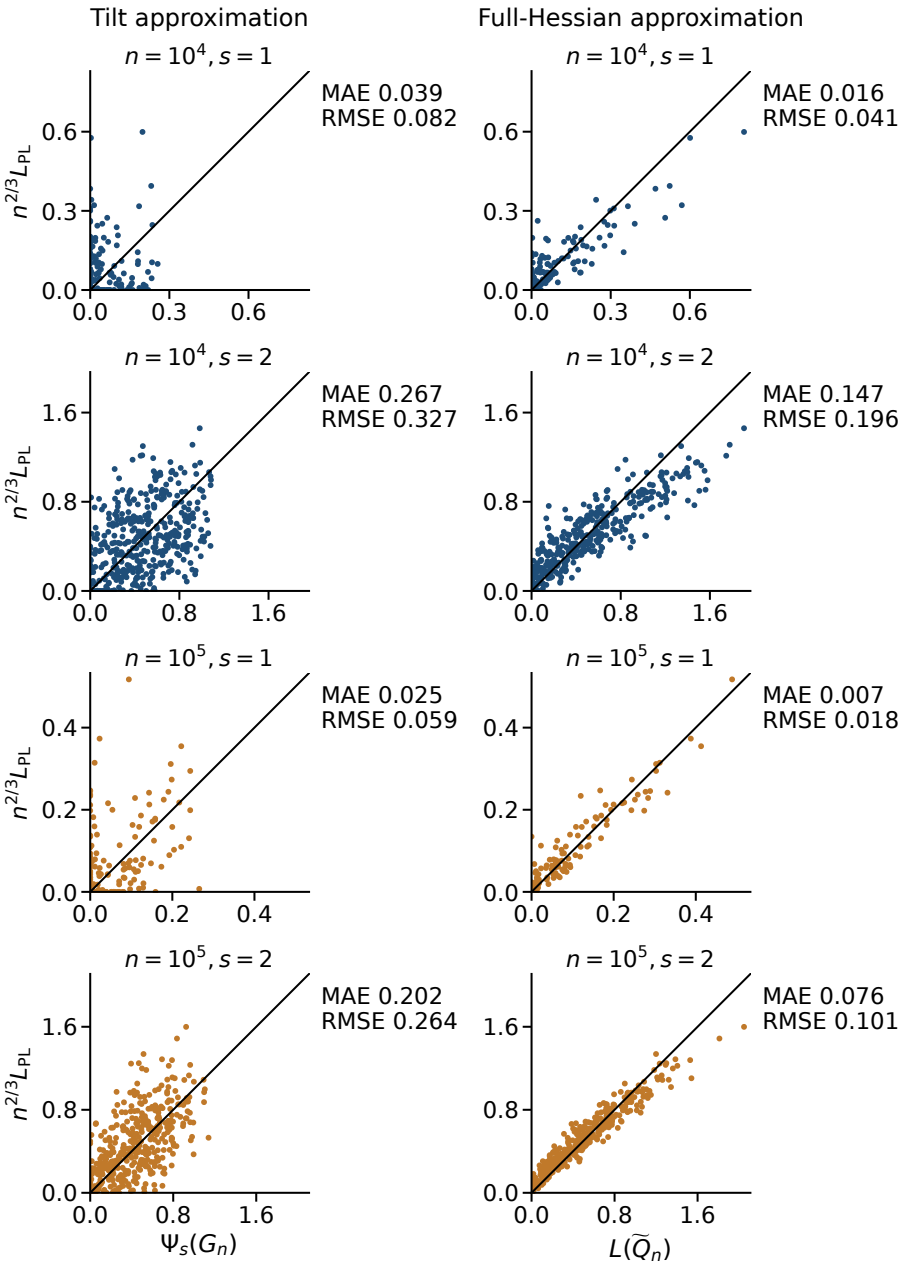


Fig. 4 Same-sample comparisons for $s > 0$. The vertical axis is the numerical scaled length. Each row corresponds to one sample-size and local-parameter pair. The horizontal axis is the tilt approximation in the left column and the full-Hessian quartic approximation in the right column. Each panel contains all 400 samples in its cell; the diagonal denotes equality. Both axes have equal scales, and the two panels in each row share the same limits. Mean absolute error (MAE) and root mean squared error (RMSE) are relative to the numerical statistic.

These observations identify random curvature as a useful finite-sample component of the local approximation, while leaving additional discrepancies to be explained. The study uses two sample sizes and one pair (q, H); it supplies a finite-sample illustration rather than an estimated convergence rate.

Different angular arrangements with a common limit.

I next use the circular family of Section 6, with $H = \lambda = 1/4$, for the uniform circle, regular hexagon, and regular octagon. Each angular law is sampled independently, without balancing its vertices or symmetrizing the observations. For each $n \in \{10^4, 10^5\}$, the two fixed local parameters are $s \approx 1.51446$ and $s \approx 2.50260$, chosen to give limiting occurrence probabilities 0.3 and 0.8. There are 200 independent samples per cell, giving 2,400 samples. The design and analysis rules were fixed before the completed run.

For this experiment, let $Y_n^{\circ,\mathrm{num}} = n^{2/3} L_{\mathrm{PL}}^{\circ}$, where L_{PL}° is the raw longest positive bar of the numerical piecewise-linear field. All positive bars are retained. The field is obtained from a finite Fourier approximation to the KDE and a six-neighbour triangulation with spacing approximately $0.04n^{-1/6}$; the exterior component joins all boundary vertices. The normalization $M_s = (a_{\mathrm{circ}} s)^2/(4b_{\mathrm{circ}})$ is the largest length in the corresponding limiting law.

Figure 5 compares all three numerical distributions with that law. The empirical curves are broadly comparable across the angular arrangements, while departures from the limiting CDF remain visible. For example, at $n = 10^5$ and the larger s, the proportions exceeding $0.25M_s$ are 82/200, 83/200, and 81/200 for the circle, hexagon, and octagon. These are descriptive comparisons, not a test of finite-sample equality or an estimate of a convergence rate.

Each sample has a bound E_T for the interpolation term of the finite Fourier field; all 2,400 values satisfy $E_T < 0.056M_s$. This bound covers interpolation only; the KDE-to-Fourier approximation and floating-point evaluation errors are outside its scope. Complete threshold tables retain the preselected levels $0.1M_s$, $0.25M_s$, and $0.5M_s$, with nominal descriptive binomial intervals and interpolation-budget ambiguity counts.

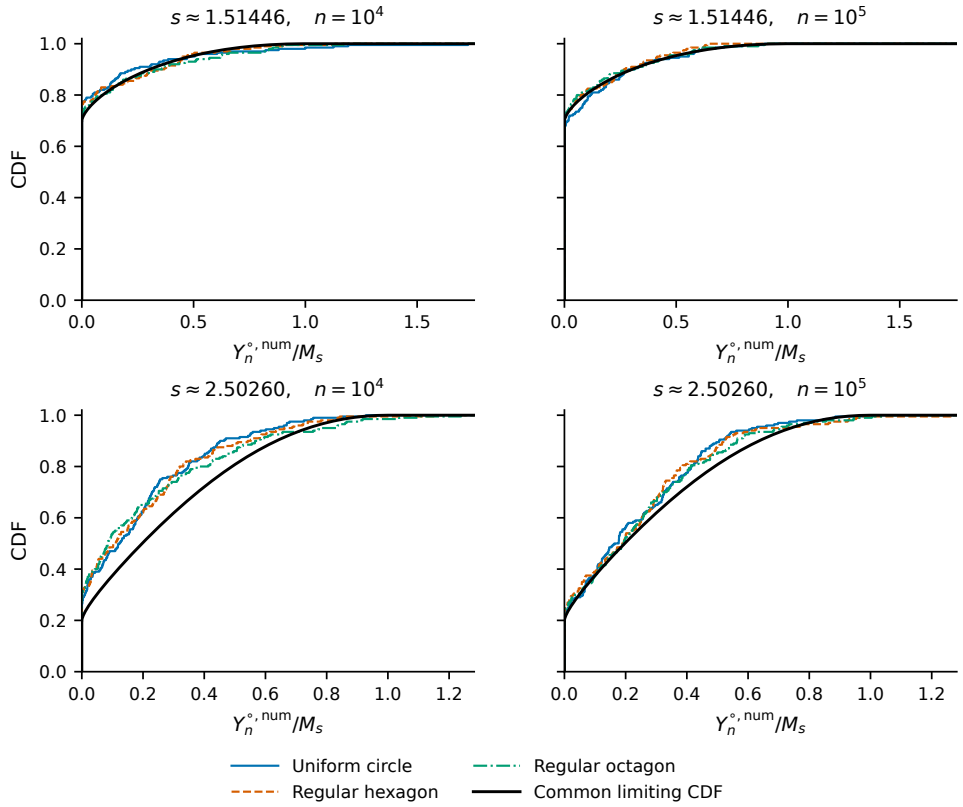


Fig. 5 Angular arrangements and the common circular-family limit. Each empirical CDF uses all 200 samples in its cell; the black curve is the common limiting CDF. Columns correspond to sample size and rows to the two local parameters. The displayed statistic is the raw numerical length $Y_n^{\circ,\mathrm{num}}/M_s$ defined in the text. All zero values and values above one are retained.

8 Statistical interpretation and further directions

The limit laws describe the survival of a shallow population loop under sampling noise at a fixed smoothing scale. Their statistical interpretation concerns the local parameter window of Theorems 2.1 and 6.1.

Substitution into the kernel sum gives, for every finite sample X and displacement c, $\widehat{f}_{X+c}(x) = \widehat{f}_X(x-c)$. Translation induces a natural isomorphism of the plane modules, so $L(X+c) = L(X)$. Theorem 2.1 therefore applies to the pure location family $f_\varepsilon(\cdot - \mu)$ without estimating μ for the full-plane statistic. The same samplewise identity applies to the circular sampling model of Theorem 6.1 translated by μ. In both cases the corresponding fixed disk is $\mu + D_\rho$.

Both theorems concern a fixed smoothing scale and fixed local parameters. The threshold formulas below refer to the Gaussian-difference model of Theorem 2.1 and its notation. For that model, $\sqrt{n}L_n \to 0$ in probability, whereas $n^{2/3}L_n$ has the stated nondegenerate law when $s > 0$.

For a fixed threshold $\tau > 0$ on the scaled length, Theorem 2.1 and the continuous part of the limiting CDF give

$$\Pr(n^{2/3} L_n > \tau) \longrightarrow \begin{cases} 1 - \exp\{-r_s(\tau)^2/(2\sigma_g^2)\}, & s > 0,\ 0 < \tau < \ell_s, \\ 0, & s \le 0 \text{ or } (s > 0,\ \tau \ge \ell_s). \end{cases}$$

The upper endpoint is included because the limit law has no atom there. A fixed positive threshold on the unscaled L_n instead has limiting exceedance probability zero for every fixed s.

The zero-threshold rule $\varphi_n = \mathbf{1}_{\{L_n > 0\}}$ uses the separate event conclusion of Theorem 2.1. Its rejection probability tends to zero along each fixed local sequence with $s \le 0$, and to $1 - \exp(-\kappa_{\mathrm{occ}} s^3)$ for $s > 0$. Thus it has pointwise asymptotic level zero within this local family. The cubic dependence is in the exponential argument. These formulas describe the topology-occurrence transition and positive scaled thresholds; calibration to a prescribed nonzero level, uniform composite-null guarantees, unknown-parameter plug-in procedures, and minimax detection bounds require separate results.

The explicit law provides a benchmark for the numerical persistence comparisons in Section 7. Relating a computed bar length to this continuous limit requires control of both discretization and finite-sample errors. Open problems include shrinking bandwidths, asymmetric perturbations, and parameter-uniform calibration, each requiring corresponding approximation and topology estimates.

Appendix A Probability estimates

This appendix supplies the probabilistic inputs for Section 5: the gradient limit, local field approximation, and localization estimates. The final subsection combines these inputs on a common event.

A.1 Population coefficients and remainder bounds

Use the model, constants, and scaled field from Sections 1–2. Write $D_\varepsilon = 1 - \varepsilon q$, $Z_n = \widehat{f}_n - m_{\varepsilon_n}$, and $D_R = \{u : |u| \le R\}$. The identity $q(1+H)^2 - (q+H)^2 = (1-q)(q-H^2) > 0$ verifies $0 < e < 1$.

I use a fixed C^j norm controlling all derivatives through order j. For $j = 2$, take the maximum of the function supremum, gradient Euclidean-norm supremum, and Hessian operator-norm supremum. Componentwise norms are equivalent, with deterministic constants. Constants in local estimates may depend on the fixed model parameters and the indicated domain or derivative order.

Completing the square in each coordinate gives $\phi_H * \phi_v = \phi_{H+v}$. Consequently $\mathbb{E}_\varepsilon \widehat{f}_n = \phi_H * f_\varepsilon = m_\varepsilon$, with $m_\varepsilon(x) = p_\varepsilon(|x|^2)$ as in Section 1. The critical identity $eB/v_2 = A_0/v_1$ gives $p_e'(0) = 0$; differentiating the displayed formula for p_ε gives $b = -p_e''(0)/2 > 0$ and the coefficient a defined there.

If $d = \varepsilon - e$, then

$$\alpha_\varepsilon := p'_\varepsilon(0) = \frac{adD_c}{D_c - qd} = ad + O(d^2), \qquad \beta_\varepsilon := \frac{1}{2}p''_\varepsilon(0) = -b + O(d). \tag{A.1}$$

These remainders are uniform on a sufficiently small fixed neighborhood of e on which $D_\varepsilon \geq D_c/2$. On that neighborhood and $0 \leq w \leq 1$, Taylor's integral formula is

$$p_\varepsilon(w) = p_\varepsilon(0) + \alpha_\varepsilon w + \beta_\varepsilon w^2 + w^3 r_\varepsilon(w), \qquad r_\varepsilon(w) = \frac{1}{2}\int_0^1 (1-t)^2 p'''_\varepsilon(tw)\, dt. \tag{A.2}$$

The functions $r_\varepsilon, r'_\varepsilon, r''_\varepsilon$ are uniformly bounded, since the first five derivatives of the two exponentials and D_ε^{-1} are bounded on this compact parameter set. The Cartesian remainder

$$\mathcal{R}_\varepsilon(x) = |x|^6 r_\varepsilon(|x|^2)$$

thus satisfies, for $j = 0, 1, 2$,

$$\|D^j \mathcal{R}_\varepsilon(x)\| \leq C|x|^{6-j}, \qquad |x| \leq 1. \tag{A.3}$$

The population mean thus has a smooth Cartesian expansion at the origin.

A.2 Gradient covariance and triangular-array CLT

The contribution of one observation to the gradient at zero is

$$Y(x) = \nabla \phi_H(-x) = \frac{x}{2\pi H^2} e^{-|x|^2/(2H)}. \tag{A.4}$$

The vector Y is bounded, odd, and rotation equivariant. Symmetry of f_ε gives $\mathbb{E}_\varepsilon Y = 0$ and an isotropic covariance matrix. To compute its diagonal entries, let X have density ϕ_v and put $\lambda = (2v)^{-1} + H^{-1}$. The Gaussian integrals

$$\int_{\mathbb{R}} e^{-\lambda x^2}\, dx = \sqrt{\pi/\lambda}, \qquad \int_{\mathbb{R}} x^2 e^{-\lambda x^2}\, dx = \frac{\sqrt{\pi}}{2\lambda^{3/2}}$$

give

$$\mathbb{E}_{\phi_v}\left[X_1^2 e^{-|X|^2/H}\right] = \frac{1}{2\pi v}\frac{\pi}{2\lambda^2} = \frac{vH^2}{(H+2v)^2}. \tag{A.5}$$

Integrating against the density f_ε from Section 1 yields

$$\begin{aligned} \mathrm{Var}_\varepsilon(Y_1) &= \frac{(H+2)^{-2} - \varepsilon q^2 (H+2q)^{-2}}{4\pi^2 H^2 D_\varepsilon} \\ &\longrightarrow \sigma_g^2 := \frac{(H+2)^{-2} - eq^2(H+2q)^{-2}}{4\pi^2 H^2 D_c}. \end{aligned} \tag{A.6}$$

Thus σ_g^2 is the variance of each coordinate of G. Since f_e is everywhere positive and $t \cdot Y$ is continuous and nonconstant for every nonzero t, its variance is positive. Hence $\mathrm{Cov}_e(Y) = \sigma_g^2 I_2$ is positive definite.

Since $\nabla m_{\varepsilon_n}(0) = 0$,

$$G_n = \frac{1}{\sqrt{n}} \sum_{i=1}^{n} Y(X_{ni}).$$

For any fixed $t \in \mathbb{R}^2$, the variables $t \cdot Y(X_{ni})$ are uniformly bounded and centered. The Lindeberg terms with threshold $\epsilon\sqrt{n}$, for any $\epsilon > 0$, vanish for all sufficiently large n. Explicitly, the Taylor remainder of e^{iz} is bounded by $|z|^3/6$, so

$$\mathbb{E} \exp\{it \cdot Y(X_{n1})/\sqrt{n}\} = 1 - \frac{\mathbb{E}(t \cdot Y(X_{n1}))^2}{2n} + O_t(n^{-3/2}).$$

Rowwise independence raises this expression to its n-th power. Its limit is $\exp(-\sigma_g^2|t|^2/2)$. The characteristic-function continuity theorem proves

$$G_n \Rightarrow G, \qquad G \sim N(0, \sigma_g^2 I_2). \tag{A.7}$$

Polar integration of this two-dimensional Gaussian density gives

$$\Pr(|G| > M) = e^{-M^2/(2\sigma_g^2)}, \qquad M \geq 0. \tag{A.8}$$

In particular, points and circles have zero Gaussian probability.

A.3 Uniform derivative moments on fixed compact sets

Lemma A.1 *For every fixed compact $K \subset \mathbb{R}^2$ and integer $j \geq 0$,*

$$\mathbb{E}\|Z_n\|_{C^j(K)}^2 \leq \frac{C_{j,K,H}}{n}. \tag{A.9}$$

The constant is uniform over all admissible row distributions from Section 1; in fact the argument works for any rowwise iid observations with this fixed kernel.

Proof Every Gaussian derivative $D^\gamma \phi_H$ is a polynomial times a Gaussian. Thus $M_\gamma := \sup_x |D^\gamma \phi_H(x)| < \infty$. Bounded derivatives of one higher order dominate the difference quotients, allowing differentiation under expectation to any fixed finite order. Consequently

$$D^\gamma Z_n(x) = \frac{1}{n} \sum_i \{D^\gamma \phi_H(x - X_{ni}) - \mathbb{E} D^\gamma \phi_H(x - X_{ni})\}, \qquad \mathbb{E}|D^\gamma Z_n(x)|^2 \leq \frac{M_\gamma^2}{n}. \tag{A.10}$$

Choose a fixed $A > 0$ with $K \subset Q_A = [-A, A]^2$, and put $I = [-A, A]$, $\ell = 2A$. For a C^1 function v on I, averaging the fundamental theorem of calculus gives the exact identity

$$v(x) = \ell^{-1} \int_I v(t)\, dt + \int_I k_x(t) v'(t)\, dt, \quad k_x(t) = \begin{cases} (t + A)/\ell, & t \leq x, \\ -(A - t)/\ell, & t > x. \end{cases} \tag{A.11}$$

Here $|k_x(t)| \le 1$. Applying this identity successively in the two coordinates gives, with all integrals over $(t,z) \in Q_A$,

$$v(x,y) = \ell^{-2} \iint v(t,z)\,dt\,dz + \ell^{-1} \iint k_x(t)\partial_1 v(t,z)\,dt\,dz \\ + \ell^{-1} \iint k_y(z)\partial_2 v(t,z)\,dt\,dz + \iint k_x(t)k_y(z)\partial_{12} v(t,z)\,dt\,dz.$$

Cauchy–Schwarz and $|Q_A| = \ell^2$ imply

$$\|v\|_\infty \le \ell^{-1}\|v\|_{L^2(Q_A)} + \|\partial_1 v\|_{L^2(Q_A)} + \|\partial_2 v\|_{L^2(Q_A)} + \ell\|\partial_{12} v\|_{L^2(Q_A)}. \tag{A.12}$$

Apply (A.12) to $D^\beta Z_n$ for every $|\beta| \le j$. By (A.10) and integration,

$$\mathbb{E}\|D^\gamma Z_n\|^2_{L^2(Q_A)} \le \ell^2 M_\gamma^2/n.$$

Squaring (A.12), using $(a_1 + \cdots + a_4)^2 \le 4\sum a_i^2$, and summing over the finitely many multiindices proves (A.9). Only derivatives through order $j+2$ enter these moment bounds; all exist and are bounded. Continuity of the sample derivatives identifies each compact supremum with a supremum over a countable dense set, proving measurability. □

I use $Q_1 = [-1,1]^2$ in the local estimates below. The constants depend on the fixed kernel variance H.

A.4 The fixed-compact C^2 approximation

Proposition A.2 *For each fixed $R < \infty$, define*

$$\Delta_{n,R} = \|F_n - Q_{s,G_n}\|_{C^2(D_R)}.$$

For all sufficiently large n,

$$\Delta_{n,R} \le C_{s,R} n^{-1/3} + C_R n^{1/3}\|Z_n\|_{C^2(Q_1)}, \qquad \mathbb{E}\Delta^2_{n,R} \le C_{s,R} n^{-1/3}. \tag{A.13}$$

In particular $\Delta_{n,R} = O_P(n^{-1/6})$, and jointly

$$(G_n, F_n|_{D_R}) \Rightarrow (G, Q_{s,G}|_{D_R}) \quad \text{in } \mathbb{R}^2 \times C^2(D_R). \tag{A.14}$$

Proof Fix R before letting $n \to \infty$, so that $n^{-1/6} D_R \subset D_1 \subset Q_1$ eventually. Equations (A.1)–(A.3) yield

$$n^{2/3}\{m_{\varepsilon_n}(n^{-1/6}u) - m_{\varepsilon_n}(0)\} = n^{1/3}\alpha_{\varepsilon_n}|u|^2 + \beta_{\varepsilon_n}|u|^4 + n^{2/3}\mathcal{R}_{\varepsilon_n}(n^{-1/6}u), \\ n^{1/3}\alpha_{\varepsilon_n} = as + O_s(n^{-1/3}), \qquad \beta_{\varepsilon_n} = -b + O_s(n^{-1/3}). \tag{A.15}$$

For each derivative order $j = 0, 1, 2$, the population remainder obeys

$$\sup_{D_R} \left\| D^j_u [n^{2/3}\mathcal{R}_{\varepsilon_n}(n^{-1/6}u)] \right\| \le C_R n^{2/3} n^{-j/6} n^{-(6-j)/6} = C_R n^{-1/3}. \tag{A.16}$$

For the centered empirical part put

$$V_n(u) = Z_n(n^{-1/6}u) - Z_n(0) - n^{-1/6}\nabla Z_n(0)\cdot u.$$

Taylor's integral formula and the chain rule give, separately at the three required derivative orders,

$$\begin{aligned} |V_n(u)| &\le \tfrac{1}{2} n^{-1/3} |u|^2 \sup_{Q_1} \|D^2 Z_n\|, \\ |\nabla_u V_n(u)| &\le n^{-1/3} |u| \sup_{Q_1} \|D^2 Z_n\|, \\ \|D_u^2 V_n(u)\| &\le n^{-1/3} \sup_{Q_1} \|D^2 Z_n\|. \end{aligned} \tag{A.17}$$

Multiplication by $n^{2/3}$ therefore bounds its full $C^2(D_R)$ norm by $C_R n^{1/3} \|Z_n\|_{C^2(Q_1)}$. Lemma A.1 makes this $O_P(n^{-1/6})$, with squared expectation $O(n^{-1/3})$. The removed linear term is exactly

$$n^{2/3} n^{-1/6} \nabla Z_n(0) \cdot u = \sqrt{n} \nabla \widehat{f}_n(0) \cdot u = G_n \cdot u.$$

More generally, a centered empirical Taylor coefficient of spatial order $j \ge 2$ has size

$$n^{2/3} n^{-j/6} D^j Z_n(0) = O_P(n^{(1-j)/6}).$$

For $j = 2, 3, 4$ these orders are $n^{-1/6}, n^{-1/3}, n^{-1/2}$, respectively; (A.17) controls the full nonlinear remainder through two derivatives.

Combining (A.15)–(A.17) proves (A.13). Continuity of $g \mapsto Q_{s,g}|_{D_R}$ into $C^2(D_R)$, the CLT (A.7), and the error tending to zero in probability give (A.14). A finite list of fixed radii is covered by applying the argument to the largest radius. □

Lemma A.3 (Empirical-Hessian approximation) *Fix q, H, s under the assumptions of Theorem 2.1, and fix $R < \infty$. Set*

$$M_n = \frac{1}{2} n^{1/3} D^2 \widehat{f}_n(0), \qquad \widetilde{Q}_n(u) = G_n \cdot u + u^\top M_n u - b|u|^4.$$

There are finite constants, depending only on the fixed parameters and R, such that for all sufficiently large admissible rows,

$$\|F_n - \widetilde{Q}_n\|_{C^2(D_R)} \le C_{q,H,s,R} n^{-1/3} + C_R n^{1/6} \|Z_n\|_{C^3(Q_1)},$$
$$\mathbb{E}\|F_n - \widetilde{Q}_n\|_{C^2(D_R)}^2 \le C_{q,H,s,R} n^{-2/3}.$$

In particular the norm is $O_P(n^{-1/3})$. Moreover,

$$\mathbb{E} M_n = \frac{asD_c}{D_c - qsn^{-1/3}} I_2, \qquad \mathbb{E} M_n - asI_2 = \frac{aqs^2 n^{-1/3}}{D_c - qsn^{-1/3}} I_2.$$

Proof Let $h = n^{-1/6}$; eventually $hD_R \subset Q_1$. Equation (A.1) and $D^2 m_\varepsilon(0) = 2\alpha_\varepsilon I_2$ give the two expectation identities. In the population expansion (A.15), the quadratic term is retained exactly. The remaining difference is

$$(\beta_{\varepsilon_n} + b)|u|^4 + n^{2/3} \mathcal{R}_{\varepsilon_n}(hu).$$

The first term has $C^2(D_R)$ norm $O_{q,H,s,R}(n^{-1/3})$. For $j = 0, 1, 2$, (A.3) gives

$$\sup_{D_R} \|D_u^j [n^{2/3} \mathcal{R}_{\varepsilon_n}(hu)]\| \le C_R n^{2/3} h^j h^{6-j} = C_R n^{-1/3}.$$

For the centered field, put

$$W_n(u) = Z_n(hu) - Z_n(0) - h \nabla Z_n(0) \cdot u - \tfrac{1}{2} h^2 u^\top D^2 Z_n(0) u.$$

With $K_n = \sup_{Q_1} \|D^3 Z_n\|$, where the tensor norm is the multilinear operator norm, Taylor's integral formula and the chain rule yield

$$|W_n(u)| \le \tfrac{1}{6} h^3 |u|^3 K_n, \quad |\nabla_u W_n(u)| \le \tfrac{1}{2} h^3 |u|^2 K_n, \quad \|D_u^2 W_n(u)\| \le h^3 |u| K_n.$$

The last bound follows directly from $D_u^2 W_n = h^2 [D^2 Z_n(hu) - D^2 Z_n(0)]$. Thus

$$n^{2/3} \|W_n\|_{C^2(D_R)} \le C_R n^{1/6} \|Z_n\|_{C^3(Q_1)}.$$

The subtracted linear term becomes $G_n \cdot u$, since $\nabla m_{\varepsilon_n}(0) = 0$, and the quadratic terms combine to $u^\top M_n u$. This proves the deterministic bound. Lemma A.1 with $j = 3$ gives $\mathbb{E}\|Z_n\|^2_{C^3(Q_1)} \le C/n$; its proof uses Gaussian derivatives through order five. Squaring the bound proves the asserted second moment. All compact norms are measurable by continuity and a countable dense subset, and G_n, M_n are continuous functions of the sample. □

The approximation retains a full symmetric matrix. Its conclusion concerns each fixed compact disk; it gives no rate for the full-plane length, its distribution, or its exact positive-bar event.

A.5 A fixed disk and the growing inner annulus

Since $p_e''(0) = -2b$, choose, before observing any sample, a fixed $0 < \rho < 1$ such that

$$\sup_{0 \le w \le \rho^2} p_e''(w) \le -3b/2. \tag{A.18}$$

Continuity in (ε, w) permits a fixed $d_0 > 0$ such that $|\varepsilon - e| \le d_0$ implies $0 < \varepsilon < 1$, $D_\varepsilon \ge D_c/2$, and $p_\varepsilon''(w) \le -b$ on the same interval. For all sufficiently large n, (A.1) then gives

$$|\alpha_{\varepsilon_n}| \le A_s n^{-1/3}, \qquad A_s = 2a|s|,$$

and, for $r = |x| \le \rho$,

$$x \cdot \nabla m_{\varepsilon_n}(x) = 2r^2 p_{\varepsilon_n}'(r^2) \le 2A_s n^{-1/3} r^2 - 2br^4. \tag{A.19}$$

Define $S_n = \sqrt{n} \sup_{D_\rho} |\nabla Z_n|$. Lemma A.1 gives $\mathbb{E} S_n^2 \le C$. If $R^2 \ge 2A_s/b$ and $Rn^{-1/6} \le r \le \rho$, the right side of (A.19) is at most $-br^4$, whereas

$$|x \cdot \nabla Z_n(x)| \le n^{-1/2} S_n r \le (S_n/R^3) r^4. \tag{A.20}$$

Thus, on $\{S_n \le bR^3/2\}$, the empirical radial derivative is at most $-br^4/2 < 0$ throughout this entire annulus. Since

$$u \cdot \nabla_u F_n(u) = n^{2/3} x \cdot \nabla_x \widehat{f}_n(x), \qquad x = n^{-1/6} u,$$

the event

$$E_{n,R} = \{u \cdot \nabla F_n(u) < 0 \text{ for all } R \le |u| \le \rho n^{1/6}\} \tag{A.21}$$

satisfies

$$\limsup_{n \to \infty} \Pr(E_{n,R}^c) \le \frac{4C}{b^2 R^6} \quad \text{for every sufficiently large fixed } R. \tag{A.22}$$

Declare the finitely many inapplicable rows failures. Taking $n \to \infty$ first, then $R \to \infty$, makes the upper bound in (A.22) vanish.

Remark At each fixed finite radius $R > 0$, the limiting field satisfies

$$\max_{|u|=R} u \cdot \nabla Q_{s,G}(u) = 2asR^2 - 4bR^4 + R|G|.$$

This maximum is positive with positive Gaussian probability, and with probability one if $4bR^3 - 2asR \le 0$. By $C^1(D_R)$ convergence and the open condition of a positive maximum, the failure probability has a positive limiting lower bound at that radius. Thus (A.22) uses the stated order of limits.

A.6 Measurable events and diagonal choice

Fix the model parameters and the physical radius ρ as in Theorem 2.1. Use $U = as$ and, for $U > 0$, the threshold t_c defined in Section 2. The exterior event $\mathcal{E}_n(\rho)$ from Lemma 4.1 is Borel by Proposition B.7 and satisfies $\Pr(\mathcal{E}_n(\rho)^c) \to 0$.

Set $\delta_k = 2^{-k}$ for $k \ge 1$. I choose deterministic parameters in the order Γ_k, R_k, η_k, n_k.

First choose $M_k \ge 1$ large and $d_k > 0$ small enough that

$$\Gamma_k = \{g : d_k \le |g| \le M_k\} \cap \begin{cases} \{g : \big||g| - t_c\big| \ge d_k\}, & U > 0, \\ \mathbb{R}^2, & U \le 0 \end{cases} \qquad \text{(A.23)}$$
$$\text{satisfies} \quad \Pr(G \notin \Gamma_k) < \delta_k/4.$$

Such a nonempty compact set exists by (A.8): the Gaussian tail vanishes as $M_k \uparrow \infty$, while the excluded neighborhoods of the origin and, for $U > 0$, the threshold circle have vanishing probability as $d_k \downarrow 0$. Its boundary is a finite union of circles of Gaussian measure zero, so (A.7) gives $\Pr(G_n \notin \Gamma_k) \to \Pr(G \notin \Gamma_k)$.

Next choose a final radius $R_k \ge R_0(\Gamma_k)$ from Theorem B.4, large enough that the bound in (A.22) is strictly less than $\delta_k/4$. For this final R_k, let $\eta_{R_k} > 0$ be the tolerance supplied by Theorem B.4, uniform over Γ_k. Choose $0 < \eta_k \le \min\{\eta_{R_k}, \delta_k/2\}$.

For rows satisfying legality, $R_k \le \rho n^{1/6}$, and the deterministic thresholds in A.4–A.5, define

$$A_{n,k} = \{G_n \in \Gamma_k\} \cap E_{n,R_k} \cap \{\Delta_{n,R_k} < \eta_k\}; \qquad \text{(A.24)}$$

set $A_{n,k} = \varnothing$ otherwise. Here E_{n,R_k} is the strict radial-derivative sign event on the entire closed annulus $R_k \le |u| \le \rho n^{1/6}$ from (A.21). For an admissible row, (A.24) is the event (B.18), so Proposition B.7 makes it Borel.

For each fixed k, (A.13) gives $\Delta_{n,R_k} \to 0$ in probability. Combining this with (A.22), (A.23), and the union bound yields

$$\limsup_n \Pr(A_{n,k}^c) \le \delta_k/2. \qquad \text{(A.25)}$$

Since $\delta_k/2 < \delta_k$, I can choose deterministic integers $n_1 \geq 1$ and $n_k \geq \max\{k, n_{k-1}+1\}$ for $k \geq 2$, incorporating all relevant deterministic thresholds, such that

$$\Pr(A_{n,k}^c) \leq \delta_k \quad \text{for every } n \geq n_k. \tag{A.26}$$

For $n \geq n_1$, let $k(n) = \max\{k : n_k \leq n\}$ and set

$$\Omega_n = A_{n,k(n)} \cap \mathcal{E}_n(\rho); \qquad \Omega_n = \varnothing \quad (n < n_1). \tag{A.27}$$

The sequence n_k is strictly increasing with $n_k \geq k$, so $k(n)$ is finite and tends to infinity. These are Borel events on the respective row sample spaces, and Lemma 4.1 together with (A.26) gives

$$\Pr(\Omega_n^c) \leq \delta_{k(n)} + \Pr(\mathcal{E}_n(\rho)^c) \longrightarrow 0. \tag{A.28}$$

Only rowwise probabilities enter this construction. On Ω_n, Proposition B.7 gives the exact zero/one-positive-bar classification on D_ρ and a natural isomorphism of its complete persistence module with that on the plane.

Appendix B Topology and perturbation stability

I establish the quartic persistence module, its stability under perturbations, and the topological facts used in Appendix A.

Throughout, k is an arbitrary fixed coefficient field and H_1 means ordinary singular homology with coefficients in k. Write $D_R = \{u \in \mathbb{R}^2 : |u| \leq R\}$ for finite R and $D_\infty = \mathbb{R}^2$. For a continuous function f on a domain D, use the increasing, closed-superlevel filtration

$$X_z(f; D) = \{u \in D : f(u) \geq -z\}, \qquad z \in \mathbb{R}.$$

All structure maps are induced by inclusion. The interval module $k_{[\alpha,\beta)}$ is nonzero for $\alpha \leq z < \beta$; a zero-length interval is the zero module. $L(f; D)$ denotes the longest finite positive H_1 bar length when this is defined, and is zero when there is no positive bar. I write c for a height, so $c = -z$. H always denotes Gaussian kernel variance; probability tolerances are denoted δ, and homotopy parameters are denoted α or θ.

B.1 Planar components and simultaneous radial retractions

Lemma B.1 (Planar component principle, with naturality) *Let A be a compact, locally contractible subset of $\mathbb{R}^2$ with finite-dimensional H_1. The dimension of $H_1(A; k)$ is the number of bounded components of $\mathbb{R}^2 \setminus A$. If $A_1 \subset A_2$ and each complement has exactly one bounded component, containing the same point p, then the inclusion $H_1(A_1; k) \to H_1(A_2; k)$ is an isomorphism.*

In particular, let f be continuous on D_R and suppose every $A_c = \{f \geq c\} \cap D_R$ is locally contractible and has finite-dimensional H_1. Every bounded component of $\mathbb{R}^2 \setminus A_c$ contains an interior local minimum of f whose value is strictly less than c. Thus no interior local minimum implies a zero H_1 module. A unique interior local minimum implies $\dim H_1(A_c; k) \leq 1$ *at every height.*

Proof The empty-set case is immediate. For nonempty A, one-point compactification and Alexander duality give the natural isomorphisms

$$\widetilde{H}_0(S^2 \setminus A; k) \cong H^1(A; k) \cong \mathrm{Hom}_k(H_1(A; k), k). \tag{B.1}$$

The open complement is locally path connected and has one component containing infinity. Its other components are bounded, giving the dimension statement. For $A_1 \subset A_2$, the complement inclusion $S^2 \setminus A_2 \to S^2 \setminus A_1$ sends $[p] - [\infty]$ to itself. Naturality in (B.1) therefore makes $H^1(A_2; k) \to H^1(A_1; k)$ an isomorphism; dualizing gives the asserted forward H_1 map. Fix an orientation of S^2. Over k, the duality and its naturality follow from the cap-product construction and the field-coefficient universal coefficient isomorphism (Hatcher 2002, §3.3).

For the last assertion, let V be a bounded component of $\mathbb{R}^2 \setminus A_c$. Any complement point on ∂D_R connects through the disk exterior to infinity, so V lies in $\operatorname{int} D_R$. Its closure is compact, $f \geq c$ on its boundary, and $f < c$ in V. The minimum on that closure is therefore attained in the open set V and is a local minimum of f. Distinct components contain distinct minima. □

Lemma B.2 (One homotopy for the entire filtration) *Let $0 < R \leq T \leq \infty$, and let f be C^1 on a neighborhood of D_T if $T < \infty$, or on $\mathbb{R}^2$ if $T = \infty$. Assume*

$$u \cdot \nabla f(u) < 0 \quad \textit{for every } R \leq |u| \leq T, \tag{B.2}$$

with no upper bound when $T = \infty$. For every real z, $X_z(f; D_R)$ is a strong deformation retract of $X_z(f; D_T)$. The retractions and homotopies commute with all filtration inclusions and induce a natural isomorphism of persistence modules.

Proof Define, simultaneously for all levels,

$$\mathcal{R}_\alpha(u) = \begin{cases} u, & |u| \leq R, \\ ((1-\alpha)|u| + \alpha R)u/|u|, & |u| \geq R, \end{cases} \qquad 0 \leq \alpha \leq 1. \tag{B.3}$$

By (B.2), moving inward increases f, so $f(\mathcal{R}_\alpha(u)) \geq f(u)$. Formula (B.3) is continuous, fixes D_R, and ends in D_R; it therefore restricts to a strong deformation retraction on every closed superlevel. Its independence of z makes the retractions and homotopies commute with all inclusions. This also holds on the plane: each point travels a finite radial segment, and the formula is jointly continuous in the Euclidean topology. In particular, if $f > 0$ and $c \leq 0$, the same homotopy retracts $\mathbb{R}^2$ onto D_R. □

The passage from component counts to persistence uses naturality. For $i : A_1 \hookrightarrow A_2$, let $j : S^2 \setminus A_2 \hookrightarrow S^2 \setminus A_1$. With a fixed sphere orientation, the Alexander duality maps $D_A : H^1(A; k) \to \widetilde{H}_0(S^2 \setminus A; k)$ satisfy

$$D_{A_1} i^* = j_* D_{A_2}.$$

This follows from the relative cap-product construction and naturality of the exact sequence of a pair (Hatcher 2002, Theorem 3.44, Corollary 3.45, pp. 254–256, and cap products, pp. 240–241). The field-coefficient universal coefficient isomorphism identifies i^* with the dual of i_* (Hatcher 2002, pp. 198–199). If both complements have one bounded component containing p, then j_* preserves the nonzero generator $[p] - [\infty]$, so i_* is an isomorphism. Thus the common minimum marks one persistent class throughout its active heights; equal dimensions alone would not identify that

class. Likewise, Lemma B.2 uses the same radial homotopy at every level, making its restrictions commute with inclusions. Separate levelwise homotopy equivalences would require this additional compatibility.

B.2 The quartic persistence module

Fix $b > 0$ and $U \in \mathbb{R}$. In the main text $U = as$. Put

$$Q_{s,g}(u) = U|u|^2 - b|u|^4 + g \cdot u.$$

Rotation is a filtration-preserving homeomorphism, so it suffices to write

$$Q(x, y) = U(x^2 + y^2) - b(x^2 + y^2)^2 + tx, \qquad t = |g| \geq 0.$$

Theorem B.3 (Exact module and length) *If $U > 0$ set*

$$t_c = \frac{4U^{3/2}}{3\sqrt{6b}}.$$

For $U > 0$ and $0 < t < t_c$, let $x_1 < x_2 < x_3$ be the three roots of $2Ux - 4bx^3 + t = 0$ and set

$$S = 3bx_1^4 - Ux_1^2, \qquad m = 3bx_2^4 - Ux_2^2.$$

The complete closed-superlevel H_1 module on $\mathbb{R}^2$ is

$$H_1(X_\bullet(Q; \mathbb{R}^2); k) \cong \begin{cases} k_{[-U^2/(4b),\, 0)}, & U > 0,\ t = 0, \\ k_{[-S,\, -m)}, & U > 0,\ 0 < t < t_c, \\ 0, & \text{otherwise.} \end{cases} \tag{B.4}$$

In the second case $S > m$ and the bar is born at the negative-side saddle and dies at the local minimum. At $t = t_c$ the module is zero at every parameter, including the collision height: there is no nonzero singleton interval. The length $\Psi_s(g)$ defined by (B.4) *is continuous in g. It also extends continuously through $U = 0$, for fixed $b > 0$.*

Proof: critical points For $t > 0$,

$$\nabla Q = (2x(U - 2br^2) + t,\ 2y(U - 2br^2)).$$

A critical point must have $y = 0$, since otherwise $U - 2br^2 = 0$ would leave first component $t \neq 0$. At a critical root x,

$$D^2Q(x, 0) = \operatorname{diag}(2U - 12bx^2,\ 2U - 4bx^2), \qquad Q(x, 0) = 3bx^4 - Ux^2. \tag{B.5}$$

For $U \leq 0$ the cubic $j(x) = 2Ux - 4bx^3 + t$ is strictly decreasing, with one positive root; both Hessian eigenvalues there are negative. This is the only critical point and is a nondegenerate maximum.

For $U > 0$ write $a_0 = \sqrt{U/(6b)}$ and $r_0 = \sqrt{U/(2b)}$. Then $j(+a_0) = t + t_c$ and $j(-a_0) = t - t_c$. If $0 < t < t_c$,

$$-r_0 < x_1 < -a_0 < x_2 < 0 < r_0 < x_3. \tag{B.6}$$

The corresponding points are respectively a saddle, a local minimum, and a maximum. If $t = t_c$, the roots are $-a_0$ (double) and $2a_0$ (simple). The former has Hessian eigenvalues 0 and $4U/3$ and nonzero x-direction third derivative $24ba_0$, so it is not a local extremum. Its height

is $-U^2/(12b)$; the maximum height is $2U^2/(3b)$. If $t > t_c$, only the positive-root maximum remains. If $t = 0$, the origin is the only critical point for $U \le 0$, a maximum with quartic degeneracy when $U = 0$. For $U > 0$, the origin is a nondegenerate minimum and the entire circle $r = r_0$ is critical, with maximum height $U^2/(4b)$.

Proof: complement components. Since $Q(u) \to -\infty$, every closed superlevel $S_c = \{Q \ge c\}$ is compact. It is semialgebraic, hence locally contractible and of finite homological type, so Lemma B.1 applies. For $t > 0$ let

$$h(r) = Ur^2 - br^4 - tr, \qquad I_c = \{r \ge 0 : h(r) < c\}. \tag{B.7}$$

The strict complement $O_c = \{Q < c\}$ meets the circle of radius $r > 0$ exactly when $h(r) < c$. A nonempty angular section is a connected open arc containing the negative axis, or the entire circle. Every point in it can be joined to $(-r, 0)$ by a path along which $\cos\theta$ does not increase. Points whose radii belong to the same interval of I_c are therefore joined through the negative axis. Distinct intervals are separated by a missing radius: there $Q \ge c$ on the entire circle, which no complement path can cross. At $r = 0$ the origin belongs to O_c exactly when $c > 0$ and then joins the adjacent radial interval. Thus complement components correspond exactly to intervals of I_c, with boundedness preserved.

If $U \le 0$ then $h'(r) < 0$. If $U > 0$ and $t \ge t_c$, $h' \le 0$ and has at most one zero, at $r = a_0$ when $t = t_c$; integration shows that h is still strictly decreasing. In either case I_c has only its unbounded interval, so there is no bounded complement component at any height. This includes the degenerate collision height itself.

If $U > 0$ and $0 < t < t_c$, h first decreases to m at $r_m = -x_2$, then increases to S at $r_S = -x_1$, and then decreases to $-\infty$. Hence $m < S$ and I_c has exactly one bounded interval precisely for

$$m < c \le S. \tag{B.8}$$

This holds for either sign of S. At $c = m$ the minimum is excluded from the strict complement; at $c = S$ the entire circle $r = r_S$ lies in S_c and separates the two complement components. Lemma B.1 gives the H_1 dimensions in (B.4).

Proof: maps and pairing. For $S \ge c_1 \ge c_2 > m$, the inclusion $O_{c_2} \subset O_{c_1}$ sends the unique bounded component, marked by $p_m = (x_2, 0)$, into the bounded component with that same marker. It also preserves the infinity component. Lemma B.1, with its naturality statement, shows that $H_1(S_{c_1}) \to H_1(S_{c_2})$ is an isomorphism. The common duality class $[p_m] - [\infty]$ gives compatible bases, identifying the module with $[-S, -m)$ and the pair with the saddle and minimum. The maximum is strictly above S: $Q(-x_1, 0) > Q(x_1, 0)$ and the only maximum is x_3.

For $t = 0$ and $U > 0$, positive levels $0 < c \le U^2/(4b)$ are annuli, with the top level equal to the circle $r = r_0$. All retract radially to that same circle by a level-independent formula. At $c = 0$ the center is filled and the set becomes a disk; lower levels are also disks. This gives $[-U^2/(4b), 0)$, including its closed birth and open death. For $U \le 0$ the radial superlevels are empty, points, or disks, so their H_1 is zero.

Proof: continuity. On $0 < t < t_c$, the simple roots depend continuously on t. As $t \downarrow 0$, $x_1 \to -r_0$ and $x_2 \to 0$, so $S - m \to U^2/(4b)$. As $t \uparrow t_c$, x_1 and x_2 coalesce at $-a_0$ and $S - m \to 0$. These limits agree with the definitions at $t = 0$ and $t = t_c$. Within the three-root regime, differentiating critical values gives

$$\frac{d}{dt}(S - m) = x_1 - x_2 < 0. \tag{B.9}$$

Thus $0 \le \Psi_s(g) \le U_+^2/(4b)$, which also proves continuity through $U = 0$. Rotation invariance makes Ψ depend on g only through the continuous map $|g|$. For fixed positive U, this proves continuity everywhere in g, although the positive-bar indicator is discontinuous on the threshold circle. □

B.3 Uniform perturbations and persistence pairing

For fixed U, b define the nondegenerate parameter region

$$\mathcal{G} = \begin{cases} \mathbb{R}^2 \setminus \big(\{0\} \cup \{|g| = t_c\}\big), & U > 0, \\ \mathbb{R}^2 \setminus \{0\}, & U \le 0. \end{cases}$$

The region $\mathcal{G}$ consists of the tilts used for the nondegenerate critical-point correspondence below; Theorem B.3 covers the remaining parameters.

Theorem B.4 (Uniform disk transfer) *Fix a nonempty compact set $\Gamma \subset \mathcal{G}$. There exist $R_0 > 0$ and $\beta > 0$ such that for **each final radius $R \ge R_0$** there is a tolerance $\eta_R > 0$ with the following property. For every $g \in \Gamma$, every finite $T \ge R$, and every function f satisfying*

1. *f is C^∞ on an open neighborhood of the closed disk D_T and its restriction to D_T is definable in an o-minimal structure;*
2. *$\|f - Q_{s,g}\|_{C^2(D_R)} < \eta_R$, where the norm controls the function, Euclidean gradient norm, and Hessian operator norm;*
3. *$u \cdot \nabla f(u) < 0$ throughout $R \le |u| \le T$,*

the H_1 filtration on D_T has exactly the following module:

$$H_1(X_\bullet(f; D_T); k) \cong \begin{cases} k_{[-S_f, -m_f)}, & U > 0,\ 0 < |g| < t_c, \\ 0, & \text{otherwise.} \end{cases} \tag{B.10}$$

In the one-bar case, m_f and S_f are the heights of the corresponding minimum and saddle. All model critical points and all critical points of f in D_T lie in $\operatorname{int} D_R$, with matching Morse indices and height order. The choice also guarantees

$$\max_{\partial D_R} f < \min_i c_i(f) - 2\beta, \qquad \max_{\partial D_T} f \le \max_{\partial D_R} f. \tag{B.11}$$

For $\omega = \|f - Q_{s,g}\|_{C^0(D_R)}$, every corresponding critical height satisfies

$$|c_i(f) - c_i(Q_{s,g})| \le \omega. \tag{B.12}$$

Consequently $|S_f - S| \le \omega$, $|m_f - m| \le \omega$ in the one-bar case, and

$$|L(f; D_T) - \Psi_s(g)| \le 2\omega. \tag{B.13}$$

In item 1, definability may be replaced by the requirements that all closed superlevels on D_R and D_T are locally contractible with finite-dimensional homology and that their H_1 filtrations are finite constructible. In either formulation, f is C^∞ on a neighborhood of the full disk; the approximation is measured in C^2.

Proof: uniform choices By Theorem B.3, the critical points are nondegenerate on Γ. Their parameter–space graph is compact: Γ is compact, and the cubic equation bounds their radii. The implicit function theorem and compactness give a uniform lower bound $\lambda > 0$ on absolute Hessian eigenvalues and, at each fixed $g \in \Gamma$, uniform positive separations between distinct critical points and their heights. Label the branches by Morse index.

For $g \in \Gamma$,

$$u \cdot \nabla Q_{s,g}(u) = 2U|u|^2 - 4b|u|^4 + g \cdot u \le 2U_+|u|^2 - 4b|u|^4 + \sup_\Gamma |g|\,|u|.$$

Choose R_0 large enough to contain every model critical point strictly in its interior, to give radial decrease outside R_0, and to give, uniformly for all $R \geq R_0$,

$$\max_{\partial D_R} Q_{s,g} < \min_i c_i(Q_{s,g}) - 4\beta. \tag{B.14}$$

The quartic term dominates uniformly, while the model critical heights remain bounded. Fix this final R for the choice of η_R.

Around each $p_i(g)$, choose disjoint closed balls contained in $\operatorname{int} D_R$, with one sufficiently small uniform radius r_*. For $A_i = D^2 Q_{s,g}(p_i)$, arrange

$$\sup_{|u-p_i| \leq r_*} \|A_i^{-1}(D^2 Q_{s,g}(u) - A_i)\| \leq \tfrac{1}{4}.$$

For sufficiently small η_R, the map $u \mapsto u - A_i^{-1}\nabla f(u)$ is a 1/2-contraction and $\|A_i^{-1}\nabla f(p_i)\| \leq r_*/2$, so it maps the ball into itself. Its unique fixed point is the unique critical point there. Compactness gives a uniform positive lower bound for $|\nabla Q_{s,g}|$ on D_R outside these balls. Reducing η_R excludes further critical points, while the Hessian gaps preserve the indices. Item 3 excludes critical points throughout the remaining annulus.

The same bounds hold on D_R for $f_\theta = Q_{s,g} + \theta(f - Q_{s,g})$, $0 \leq \theta \leq 1$. Its critical points $p_i(\theta)$ continue uniquely and C^1 in θ, and

$$\frac{d}{d\theta} f_\theta(p_i(\theta)) = (f - Q_{s,g})(p_i(\theta)),$$

because ∇f_θ vanishes there. Integration proves (B.12). Taking η_R smaller than the critical-height gaps and β preserves the height order and turns (B.14) into the first inequality in (B.11). The second follows ray by ray from item 3.

Proof: the module and saddle attachment. Lemma B.2 naturally identifies the D_T and D_R modules. The finiteness and local-contractibility conditions, supplied by item 1 as explained in Proposition B.6, allow Lemma B.1 to be applied to $A_c = \{f \geq c\} \cap D_R$ at every height.

In the one-maximum case there is no interior minimum, hence no bounded complement component and no H_1. In the three-critical-point case, let p_m, p_S, p_M be the corresponding minimum, saddle, and maximum, with heights $m_f < S_f < M_f$. Any bounded complement component must contain p_m, so at every level there is at most one. For $c \leq m_f$ none exists. The boundary gap puts all relevant levels $c > m_f$ away from disk-boundary events.

Immediately above m_f, the Morse form $f = m_f + v_1^2 + v_2^2$ creates a bounded strict-sublevel component around p_m, isolated by a local circle of higher value. On a compact band without critical points, the flow of $\nabla f/|\nabla f|^2$ preserves the component structure. Condition (B.11) keeps each relevant band away from the disk boundary, so the smoothness and compact-band hypotheses of Milnor (1963, Lemma 2.2 and Theorems 3.1–3.2) hold.

Crossing the maximum, with local form $f = M_f - v_1^2 - v_2^2$, fills a disk along a connected punctured disk or annulus and cannot merge distinct components. At the saddle, $f = S_f + v_1^2 - v_2^2$ joins two descending branches. Above the disk maximum the complement is all of $\mathbb{R}^2$, so the component born at p_m must have merged with the exterior. The unique saddle is the only event that can make this merger; its descending branches therefore lie in the bounded p_m component and the exterior component. This identifies the attachment.

At $c = S_f$ the bounded component remains in the strict complement. Otherwise a path from p_m to the disk exterior within that complement would have a compact disk portion on which $\max f < S_f$. It would already connect the two components at some $c < S_f$, a contradiction. At $c = m_f$, Lemma B.1 excludes a bounded component. Thus the active heights are exactly $m_f < c \leq S_f$. The common markers p_m and infinity give isomorphisms of all internal H_1 maps by Lemma B.1, proving (B.10) with its stated endpoints and saddle–minimum pairing. Equation (B.12) gives (B.13). □

The choices are uniform over Γ for each final R. At $|g| = t_c$, arbitrarily small changes of the tilt give a positive bar on one side and no bar on the other, so a fixed positive perturbation tolerance cannot preserve the exact existence classification across that threshold.

B.4 Stability and definition of the statistic

These arguments serve distinct purposes. Proposition B.6 defines the statistic for every finite sample, including degenerate configurations: function triangulation gives finite constructibility and local contractibility, while radial retraction identifies the plane and disk modules. Theorem B.4 establishes the exact zero/one-bar classification and pairing on a compact nondegenerate parameter set. It uses C^2 approximation, the full annular sign, and boundary isolation, retaining C^∞ regularity on a neighborhood of the full disk. Definability is a sufficient framework, with the finite-topology alternative stated there; neither it nor the chosen regularity is asserted to be minimal. Lemma B.5 gives the elementary longest-length form of persistence stability through its direct interleaving argument. A C^0 bound permits short additional bars, so the existence probability uses the exact classification instead. The continuous enclosing radius $T(X)$ in Proposition B.7 is a convenient construction for Borel measurability, not a necessity claim.

Lemma B.5 (Elementary longest-length bound) *Suppose f and h are functions on the same domain D whose H_1 filtrations have finite interval decompositions and no infinite bars. If $\|f - h\|_\infty \le \omega$, then*

$$|L(f; D) - L(h; D)| \le 2\omega. \tag{B.15}$$

Proof The set inclusions give $X_z(f) \subset X_{z+\omega}(h) \subset X_{z+2\omega}(f)$. If f has a bar $[a, b)$ longer than 2ω, choose $a < r < s < b$ with $s - r > 2\omega$. The nonzero structure map from r to s factors as

$$H_1(X_r(f)) \longrightarrow H_1(X_{r+\omega}(h)) \longrightarrow H_1(X_{s-\omega}(h)) \longrightarrow H_1(X_s(f)).$$

The nonzero middle map forces a bar of h of length at least $s - r - 2\omega$. Let $r \downarrow a$ and $s \uparrow b$; finiteness of the decomposition gives $L(h; D) \ge b - a - 2\omega$. If $L(f; D) \le 2\omega$, the same one-sided inequality follows from nonnegativity. Exchanging f and h proves (B.15). The argument uses only the stated finite decompositions over k, on the common domain D. □

Proposition B.6 (Finite Gaussian samples) *Fix $H > 0$ and $n \ge 1$. For every ordered sample $X = (X_1, \dots, X_n) \in (\mathbb{R}^2)^n$, let*

$$\widehat{f}_X(x) = \frac{1}{n} \sum_{i=1}^{n} \phi_H(x - X_i), \qquad \phi_H(x) = \frac{1}{2\pi H} e^{-|x|^2/(2H)}.$$

The full-plane closed-superlevel H_1 module has finitely many bars, all finite, with the closed-birth/open-death convention above. The same holds on any fixed closed disk. Its longest length $L(X)$ is defined for every sample and obeys

$$|L(X) - L(Y)| \le \frac{2C_K}{n} \sum_{i=1}^{n} |X_i - Y_i|, \qquad C_K = \frac{e^{-1/2}}{2\pi H^{3/2}}. \tag{B.16}$$

In particular, the longest-bar statistic is continuous, Borel measurable, and permutation invariant on the sample space, including samples with degenerate critical points.

Proof: compact finite constructibility For each fixed sample and finite disk, the Gaussian sum is analytic on a neighborhood of a surrounding compact box. Rescaling that box to $[-1,1]^2$ makes its restriction definable in the o-minimal structure $\mathbb{R}_{\mathrm{an}}$ (van den Dries and Miller 1996, §2.5). The sample centers enter as real parameters.

Apply Coste (1999, Theorem 4.5) to the continuous definable function $-\widehat{f}_X$ on D_T. It gives one definable homeomorphism from a finite simplicial complex to D_T under which the function is affine on every simplex.

For a piecewise-affine function q on a finite complex, retract $\{q \le a\}$ to the subcomplex spanned by the vertices with $q(\text{vertex}) \le a$. For each point in $\{q \le a\}$, set its barycentric coordinates at higher vertices to zero and normalize the remaining coordinates. Linear interpolation to this point stays in $\{q \le a\}$, and the formulas agree on faces. Between successive vertex values the formula and target subcomplex are unchanged, so these retractions commute with inclusions. At a vertex value, equal-height vertices are included. The module is therefore finite-dimensional, finite constructible, and right-continuous. Decomposing the resulting finite sequence of vector spaces gives bars $[\alpha, \beta)$. The terminal disk has $H_1 = 0$, so every bar is finite. Definable triangulation, or the local conic structure theorem (Coste 1999, Theorem 4.10), also makes every superlevel locally contractible. These facts justify the use of definability in Theorem B.4.

Proof: the plane for every sample. Choose $T > \max_i |X_i|$. For $|x| \ge T$,

$$x \cdot \nabla \widehat{f}_X(x) = -\frac{1}{nH} \sum_i x \cdot (x - X_i)\phi_H(x - X_i) < 0, \tag{B.17}$$

because $x \cdot (x - X_i) \ge |x|(|x| - |X_i|) > 0$. Lemma B.2 naturally identifies the full-plane module with the finite disk module at every real height, including $c \le 0$, where the superlevels are $\mathbb{R}^2$ and D_T. The positive minimum on D_T shows that H_1 has already vanished at sufficiently low positive heights. This defines the statistic for every sample, independently of the enclosing radius and of any probability event.

Proof: continuity. Direct maximization of $|\nabla \phi_H(x)|$ gives C_K in (B.16). The mean value inequality yields

$$\|\widehat{f}_X - \widehat{f}_Y\|_{\infty,\mathbb{R}^2} \le \frac{C_K}{n} \sum_i |X_i - Y_i|.$$

The finite decompositions just proved allow Lemma B.5 to be applied on the common domain $\mathbb{R}^2$, giving (B.16). The same argument applies on any fixed disk. Symmetry of the kernel sum gives permutation invariance. □

B.5 Measurable events for persistence transfer

Proposition B.7 (Persistence on measurable events) *Let L_n^D and L_n be the all-sample statistics of Proposition B.6, use F_n, G_n from Section 1, and let $\Delta_{n,R}$ be the error in Proposition A.2.*

Fix deterministic $\rho > 0$ and a nonempty compact $\Gamma \subset \mathcal{G}$. Choose a final radius R and a uniform tolerance η_R as in Theorem B.4. For a row with $\rho n^{1/6} \ge R$, define

$$\begin{aligned} A_{n,\Gamma,R,\eta} = {} & \{G_n \in \Gamma\} \cap \{\Delta_{n,R} < \eta\} \\ & \cap \{u \cdot \nabla F_n(u) < 0 \text{ throughout } R \le |u| \le \rho n^{1/6}\}, \quad 0 < \eta \le \eta_R. \end{aligned} \tag{B.18}$$

This event is Borel. On it, the D_ρ module has the exact zero/one-positive-bar classification and pairing of Theorem B.4, and

$$|n^{2/3}L_n^D - \Psi_s(G_n)| \le 2\Delta_{n,R}, \qquad \mathbf{1}_{\{L_n^D>0\}} = \begin{cases} \mathbf{1}_{\{0<|G_n|<t_c\}}, & U > 0, \\ 0, & U \le 0. \end{cases} \tag{B.19}$$

The exterior event

$$\mathcal{E}_n(\rho) = \{x \cdot \nabla \widehat{f}_n(x) < 0 \text{ for every } |x| \ge \rho\} \tag{B.20}$$

is also Borel. On it, inclusion of D_ρ induces a natural isomorphism with the full-plane module at every filtration parameter. Hence on the intersection of these events, both modules have the same bar list and (B.19) *holds with L_n in place of L_n^D.*

Proof Every F_n is C^∞ on the plane and restricted-analytic definable on each finite disk. Thus (B.18) supplies all hypotheses of Theorem B.4 with $f = F_n$ and $T = \rho n^{1/6}$. In the one-bar regime, (B.10)–(B.12) give the saddle–minimum interval $[-S_f, -m_f)$, with each endpoint error at most $\|F_n - Q_{s,G_n}\|_{C^0(D_R)} \le \Delta_{n,R}$. Equation (B.11) gives the boundary height gap. Spatial dilation identifies the physical disk with D_T, while subtracting $\widehat{f}_n(0)$ translates the filtration and multiplying heights by $n^{2/3}$ scales bar lengths. The zero/one-bar classification therefore gives (B.19).

For fixed n, R, G_n is continuous in the sample, and the derivatives defining $\Delta_{n,R}$ are jointly continuous in sample and location. Taking norm suprema over D_R preserves continuity. The sign condition in (B.18) is a maximum strictly below zero over the deterministic compact annulus. Since Γ is compact, (B.18) is Borel. For rows with $\rho n^{1/6} < R$, set the event empty; the statistics retain their values from Proposition B.6.

For (B.20), set $T(X) = \max\{\rho, 1 + \max_i |X_i|\}$. Equation (B.17) gives the required sign for $|x| \ge T(X)$, so (B.20) is equivalent to

$$\min_{\rho \le |x| \le T(X)} [-x \cdot \nabla \widehat{f}_X(x)] > 0.$$

Writing $x = [\rho + \alpha(T(X) - \rho)]\theta$, with $(\alpha, \theta) \in [0,1] \times S^1$, expresses this minimum over a fixed compact parameter space. The integrand is jointly continuous, including when $T(X) = \rho$, so its minimum is continuous in X. This proves Borel measurability. Lemma B.2 supplies a single radial homotopy compatible with every filtration inclusion, including at density heights $c \le 0$, and hence the asserted natural isomorphism. □

On the intersection of the events in Proposition B.7, whenever $L_n > 0$, write the unique bar as $[z_n^b, z_n^d)$. Set $a_n = n^{2/3}$ and $c_n = \widehat{f}_n(0)$. Spatial dilation gives

$$X_w(F_n; D_{\rho n^{1/6}}) \cong X_{w/a_n - c_n}(\widehat{f}_n; D_\rho).$$

Consequently its rescaled endpoints are $a_n(z_n^b + c_n)$ and $a_n(z_n^d + c_n)$, preserving closed birth and open death. Each differs from its model counterpart $-S(G_n)$ or $-m(G_n)$ by at most $\Delta_{n,R}$. Endpoints expressed as density heights instead subtract c_n and correspond to S, m. For fixed $s > 0$, Theorem 2.1 gives a positive limiting probability of no positive bar. Thus the endpoints of a positive bar do not yet define an unconditional $\mathbb{R}^2$-valued random variable. Such a formulation requires an explicit absence state or marking convention; a conditional formulation must specify its conditioning event.

Appendix C Proof for angular moment designs

The circular model is treated in three stages: the local random-field approximation, exterior localization, and persistence transfer using Appendix B.

Throughout this appendix the sampling model and constants are those of Section 6. Put

$$\begin{aligned} F_n^\circ(u) &= n^{2/3}\{\widehat{f}_n^\circ(n^{-1/6}u) - \widehat{f}_n^\circ(0)\}, \\ G_n^\circ &= \sqrt{n}\nabla\widehat{f}_n^\circ(0), \qquad \Delta_{n,R}^\circ = \|F_n^\circ - Q_{s,G_n^\circ}^\circ\|_{C^2(D_R)}. \end{aligned} \tag{C.1}$$

The norm is the maximum of the function supremum, gradient Euclidean-norm supremum, and Hessian operator-norm supremum. All limits concern sufficiently large rows with $\theta_n > 0$; finitely many earlier rows can be assigned arbitrary admissible laws.

C.1 Population coefficients and the gradient

Gaussian convolution, including direct kernel integration when $\lambda = 0$, gives the population smoother

$$\begin{aligned} m_\theta(r\omega) &= C_\theta e^{-r^2/(2v)} F_\omega(z), \quad C_\theta = \frac{e^{-\theta/(2v)}}{2\pi v}, \\ F_\omega(z) &= \mathbb{E}_\nu e^{zU}, \qquad\qquad U = \omega\cdot S, \qquad z = \frac{\sqrt{\theta}\, r}{v}, \quad |\omega| = 1. \end{aligned} \tag{C.2}$$

Condition (6.1) gives $\mathbb{E}U^2 = 1/2$ and $\mathbb{E}U^4 = 3/8$. Central symmetry removes every odd moment. Consequently

$$\begin{aligned} m_\theta(x) - m_\theta(0) &= A_\theta|x|^2 + B_\theta|x|^4 + \mathcal{R}_\theta(x), \\ A_\theta &= C_\theta\frac{\theta - 2v}{4v^2}, \\ B_\theta &= C_\theta\left(\frac{1}{8v^2} - \frac{\theta}{8v^3} + \frac{\theta^2}{64v^4}\right), \\ \|D^j\mathcal{R}_\theta(x)\| &\le C|x|^{6-j}, \qquad j = 0,1,2, \quad |x| \le 1. \end{aligned} \tag{C.3}$$

The bounds are uniform on a fixed compact neighborhood of $e_{\mathrm{circ}} > 0$: Gaussian derivatives through order six are bounded, and symmetry removes degree five. Taylor's integral remainder applies also to the derivatives. Thus

$$A_{e_{\mathrm{circ}}} = 0, \quad A'_{e_{\mathrm{circ}}} = a_{\mathrm{circ}}, \quad B_{e_{\mathrm{circ}}} = -b_{\mathrm{circ}}, \qquad \begin{cases} n^{1/3}A_{\theta_n} = a_{\mathrm{circ}}s + O_s(n^{-1/3}), \\ B_{\theta_n} = -b_{\mathrm{circ}} + O_s(n^{-1/3}). \end{cases} \tag{C.4}$$

The weighted covariance follows by conditioning on S. Completing squares yields

$$\mathbb{E}[XX^\top e^{-|X|^2/H} \mid S] = e^{-\theta/(Hd)}\left(\frac{\lambda}{d^2}I_2 + \frac{\theta}{d^3}SS^\top\right). \tag{C.5}$$

For $\lambda > 0$, the tilted Gaussian has total mass $d^{-1}e^{-\theta/(Hd)}$, mean $\sqrt{\theta}S/d$, and covariance $(\lambda/d)I_2$. Direct substitution proves the same identity at $\lambda = 0$. Averaging now uses $\mathbb{E}SS^\top = I_2/2$; this step establishes isotropy despite the radial weight. The gradient summand

$$Y(X) = \nabla\phi_H(-X) = \frac{X}{2\pi H^2}e^{-|X|^2/(2H)}$$

has mean zero by central symmetry. Its per-coordinate variance is

$$\frac{e^{-\theta/(Hd)}}{8\pi^2H^4}\left(\frac{2\lambda}{d^2} + \frac{\theta}{d^3}\right),$$

which tends to (6.4). Fixed H makes Y uniformly bounded, so the rowwise triangular array satisfies Lindeberg's condition. Its covariance converges to the positive matrix $\sigma^2_{\mathrm{circ}}I_2$, proving

$$G^\circ_n \Rightarrow G^\circ \sim N(0, \sigma^2_{\mathrm{circ}}I_2). \tag{C.6}$$

This argument uses probability measures, not an input density, at $\lambda = 0$.

C.2 The compact approximation

Let $Z^\circ_n = \widehat{f}^\circ_n - m_{\theta_n}$. The proof of Lemma A.1 applies to any rowwise iid law: bounded Gaussian derivatives give pointwise variances $O(n^{-1})$, and the two-dimensional integration inequality (A.12) gives

$$\mathbb{E}\|Z^\circ_n\|^2_{C^j(K)} \le C_{j,K,H}/n \tag{C.7}$$

on each fixed compact set. Differentiation under expectation is justified by bounded derivatives of one higher order; compact suprema are measurable by continuity.

Fix R, put $h = n^{-1/6}$, and take n large enough that $hD_R \subset [-1,1]^2$. For $j = 0, 1, 2$, the scaled population remainder is bounded by

$$\sup_{D_R}\|D^j_u[n^{2/3}\mathcal{R}_{\theta_n}(hu)]\| \le C_R n^{2/3}h^j h^{6-j} = C_R n^{-1/3}.$$

For $V_n(u) = Z^\circ_n(hu) - Z^\circ_n(0) - h\nabla Z^\circ_n(0)\cdot u$ and $K_n = \sup_{[-1,1]^2}\|D^2Z^\circ_n\|$, Taylor's formula gives

$$|V_n(u)| \le h^2|u|^2K_n/2, \qquad |\nabla V_n(u)| \le h^2|u|K_n, \qquad \|D^2V_n(u)\| \le h^2K_n.$$

After multiplication by $n^{2/3}$, the squared expected C^2 norm is $O_R(n^{2/3}/n)$. The removed linear term is exactly $G^\circ_n \cdot u$, since $\nabla m_{\theta_n}(0) = 0$. Together with (C.4), this proves

$$\mathbb{E}(\Delta^\circ_{n,R})^2 \le C_{s,R}n^{-1/3}. \tag{C.8}$$

The fixed-compact process limit follows jointly with (C.6) by continuity of $g \mapsto Q^\circ_{s,g}|_{D_R}$.

C.3 Radial decrease outside a fixed disk

At $\theta = e_{\mathrm{circ}}$, write $m_j = \mathbb{E}U^j$. Since $|U| \le 1$, the moment series is absolutely differentiable and

$$zF_\omega(z) - 2F'_\omega(z) = \sum_{j\ge 0}\left(m_{2j} - \frac{2m_{2j+2}}{2j+1}\right)\frac{z^{2j+1}}{(2j)!} \ge \frac{z^3}{8} \qquad (z>0). \tag{C.9}$$

The zero-order coefficient vanishes. For $j \ge 1$, $m_{2j+2} \le m_{2j}$ and $m_{2j} > 0$, so all remaining coefficients are positive; $m_2 = 1/2$, $m_4 = 3/8$ give the displayed first term. Differentiating (C.2) therefore gives

$$-x\cdot\nabla m_{e_{\mathrm{circ}}}(x) \ge 4b_{\mathrm{circ}}r^4 e^{-r^2/(2v)} > 0 \qquad (r=|x|>0).$$

Preselect $0<\rho<1$ sufficiently small for the inner estimate in Subsection C.4. Bound the component radii by B on a fixed positive parameter neighborhood. Compactness preserves a strictly negative population margin on $\rho \le r \le 2B+1$ after shrinking this neighborhood. For $r \ge 2B$, every component satisfies $x\cdot(x-\sqrt{\theta}S) \ge r^2/2$, and Jensen's inequality gives $F_\omega(z) \ge 1$. Combining the overlapping regions yields

$$-x\cdot\nabla m_\theta(x) \ge c_\rho r^2 e^{-r^2/(2v)}, \qquad r \ge \rho. \tag{C.10}$$

The parameter neighborhood is chosen after ρ.

When $\lambda = 0$, every observation lies in D_B. On $\rho \le r \le B+1$, equation (C.7) transfers the fixed population margin with failure probability $O(n^{-1})$. For $r > B$, every kernel has strictly negative radial derivative. The overlap covers the boundary $r = B$.

Suppose $\lambda > 0$. Choose $0 < \eta_{\mathrm{env}} < H/2$ and put $u_0 = \lambda + \eta_{\mathrm{env}}$, $w = u_0 + H/2 < v$. Completing squares for $|\mu| \le B$ gives

$$\phi_\lambda(x-\mu) \le \frac{u_0}{\lambda}e^{B^2/(2\eta_{\mathrm{env}})}\phi_{u_0}(x).$$

Hence the input density satisfies $f_\theta \le C\phi_{u_0}$. For $\xi_x(X) = x\cdot\nabla\phi_H(x-X)$, the identity $\phi_H^2 = (4\pi H)^{-1}\phi_{H/2}$ and

$$\phi_{H/2}(y)\phi_{u_0}(x-y) = \phi_w(x)\phi_{t_0}(y-\alpha_0 x), \qquad \alpha_0 = \frac{H}{2w}, \quad t_0 = \frac{u_0 H}{2w},$$

and $|\xi_x(X)|^2 \le r^2H^{-2}|x-X|^2\phi_H(x-X)^2$ yield

$$\mathbb{E}\xi_x(X)^2 \le Cr^2\phi_w(x)(\alpha_0^2 r^2 + 2t_0).$$

Here the Gaussian integral of the squared norm is $\alpha_0^2 r^2 + 2t_0$. Consequently

$$\operatorname{Var}\xi_x \le Cr^2(1+r^2)e^{-r^2/(2w)}, \qquad |\xi_x - \mathbb{E}\xi_x| \le Cr. \tag{C.11}$$

Choose $2u_0 < \gamma < 2v$ and set $R_n^{\mathrm{out}} = \sqrt{\gamma \log n}$, $\kappa = 1 - \gamma/(2v) > 0$, and $\tau(r) = c_\rho r^2 e^{-r^2/(2v)}/2$. The two Bernstein exponents for a deviation $\tau(r)$ are bounded below on $\rho \le r \le R_n^{\mathrm{out}}$ by positive multiples of

$$n\frac{r^2}{1+r^2}e^{-r^2[1/v-1/(2w)]}, \qquad nre^{-r^2/(2v)}. \tag{C.12}$$

Since $0 < 1/v - 1/(2w) < 1/(2v)$, both are at least cn^κ. An n^{-2}-net has at most $Cn^4 \log n$ points. The spatial derivative of $x \cdot \nabla Z_n^\circ(x)$ is bounded deterministically by $C(1 + R_n^{\mathrm{out}})$, whereas $\min \tau \ge cn^{-\gamma/(2v)}$ and $|\partial_r \log \tau| \le 2/\rho + R_n^{\mathrm{out}}/v$. Thus interpolation and threshold variation turn a net deviation at most τ into an off-net deviation at most $3\tau/2$ for large n, below the population signal 2τ.

The same density envelope gives

$$\Pr\{\max_i |X_{ni}| > R_n^{\mathrm{out}}\} \le Cn^{1-\gamma/(2u_0)} \longrightarrow 0.$$

On its complement every kernel decreases for $r > R_n^{\mathrm{out}}$; the closed net annulus already includes equality. Therefore, in either case $\lambda = 0$ or $\lambda > 0$, the event

$$\mathcal{E}_n^\circ(\rho) = \{x \cdot \nabla \widehat{f}_n^\circ(x) < 0 \text{ for every } |x| \ge \rho\} \tag{C.13}$$

has probability tending to one. For $\lambda > 0$, one sufficient failure bound is $Cn^4 \log n \exp(-cn^\kappa) + Cn^{1-\gamma/(2u_0)}$.

C.4 The connecting inner annulus

Choose ρ so the derivative remainder in (C.3) is at most $b_{\mathrm{circ}} r^4$ after multiplication by r, and then shrink the parameter neighborhood so $B_\theta \le -3b_{\mathrm{circ}}/4$. Equations (C.3)–(C.4) give

$$x \cdot \nabla m_{\theta_n}(x) \le C_s n^{-1/3} r^2 - 2b_{\mathrm{circ}} r^4 \qquad (r \le \rho).$$

Let $S_n = \sqrt{n} \sup_{D_\rho} |\nabla Z_n^\circ|$, so $\mathbb{E}S_n^2 \le C$. For $R^2 \ge C_s/b_{\mathrm{circ}}$ and $Rn^{-1/6} \le r \le \rho$, the population term is at most $-b_{\mathrm{circ}} r^4$, and $|x \cdot \nabla Z_n^\circ(x)| \le S_n r^4/R^3$. On $\{S_n \le b_{\mathrm{circ}} R^3/2\}$ the total derivative is strictly negative. Consequently

$$\begin{aligned} E_{n,R}^\circ &= \{u \cdot \nabla F_n^\circ(u) < 0 \text{ for all } R \le |u| \le \rho n^{1/6}\}, \\ \limsup_{n\to\infty} \Pr((E_{n,R}^\circ)^c) &\le \frac{4C}{b_{\mathrm{circ}}^2 R^6}. \end{aligned} \tag{C.14}$$

Here $u \cdot \nabla F_n^\circ(u) = n^{2/3} x \cdot \nabla \widehat{f}_n^\circ(x)$ for $x = n^{-1/6}u$. Inapplicable early rows are failures. The bound is used with $n \to \infty$ first and then $R \to \infty$.

C.5 Measurable transfer and the two limits

Proposition B.6 defines the actual finite barcode and continuous longest-length statistic for every ordered finite Gaussian sample, including singular sampling and repeated

points. Write $L_n^{\circ,D}$ for this statistic on D_ρ. Its definition, like that of L_n°, applies to every sample, including outside the events used below.

Fix a nonempty compact tilt set Γ avoiding 0 and, when $s > 0$, the circle $|g| = t_{\mathrm{circ}}(s)$. Apply Theorem B.4 with $U = a_{\mathrm{circ}}s$ and $b = b_{\mathrm{circ}}$. Choose a final $R \geq R_0(\Gamma)$ also large enough for (C.14), then $0 < \eta \leq \eta_R$. For admissible rows with $T_n = \rho n^{1/6} \geq R$, define

$$A_n^\circ(\Gamma, R, \eta) = \{G_n^\circ \in \Gamma\} \cap \{\Delta_{n,R}^\circ < \eta\} \cap E_{n,R}^\circ; \tag{C.15}$$

otherwise set it empty. Each F_n° is C^∞ on a neighborhood of D_{T_n} and restricted-analytic definable there. The norm bound and the entire closed-annulus sign supply the other two hypotheses of Theorem B.4. Its model boundary estimate (B.14), the C^0 error, and the critical-height bound (B.12) give the inner boundary gap (B.11); radial decrease carries it to ∂D_{T_n}. The theorem supplies the actual saddle–minimum pairing and exact zero/one-bar classification, with closed birth and open death.

On $\mathcal{E}_n^\circ(\rho)$, Lemma B.2 gives one level-independent radial deformation from the plane to D_ρ, compatible with every filtration inclusion. Spatial dilation and the height change $z \mapsto n^{2/3}(z + \widehat{f}_n^\circ(0))$ preserve the endpoint convention. Thus the deterministic argument of Proposition B.7, now applied to (C.1), gives on $A_n^\circ \cap \mathcal{E}_n^\circ(\rho)$

$$\begin{aligned} L_n^\circ = L_n^{\circ,D}, \qquad & |n^{2/3}L_n^\circ - \Psi_s^\circ(G_n^\circ)| \leq 2\Delta_{n,R}^\circ, \\ \mathbf{1}_{\{L_n^\circ > 0\}} = & \begin{cases} \mathbf{1}_{\{0<|G_n^\circ|<t_{\mathrm{circ}}(s)\}}, & s > 0, \\ 0, & s \leq 0. \end{cases} \end{aligned} \tag{C.16}$$

The natural isomorphism identifies the empirical plane and disk modules; the model supplies their approximating endpoints.

Both events are Borel. For (C.15), all norm and sign suprema are over fixed compact sets with integrands jointly continuous in sample and position. For (C.13), put $T(X) = \max\{\rho, 1 + \max_i |X_i|\}$. Beyond $T(X)$ every kernel decreases. Parametrizing the remaining annulus by $x = [\rho + t(T(X) - \rho)]\omega$, $(t, \omega) \in [0, 1] \times S^1$, makes its strict sign a condition on a continuous maximum over a fixed compact space. This includes $T(X) = \rho$.

The diagonal construction of Appendix A.6 uses the new probability bounds as follows. For $\delta_k = 2^{-k}$, choose a nonempty compact Γ_k with Gaussian-null boundary and $\Pr(G^\circ \notin \Gamma_k) < \delta_k/4$. Such sets are obtained by bounding $|g|$ above and excluding small neighborhoods of zero and, if applicable, the threshold circle. Choose the final R_k so the bound in (C.14) is below $\delta_k/4$ and Theorem B.4 applies. Then take $0 < \eta_k \leq \min\{\eta_{R_k}, \delta_k/2\}$. Equations (C.6) and (C.8) imply

$$\limsup_n \Pr\{A_n^\circ(\Gamma_k, R_k, \eta_k)^c\} \leq \delta_k/2.$$

The strict budget slack permits deterministic increasing integers $n_k \geq k$, incorporating legality and radius thresholds, for which the same failure probability is at most δ_k for

every $n \geq n_k$. Set $k(n) = \max\{k : n_k \leq n\}$ and

$$\Omega_n^\circ = A_n^\circ(\Gamma_{k(n)}, R_{k(n)}, \eta_{k(n)}) \cap \mathcal{E}_n^\circ(\rho), \qquad \Pr((\Omega_n^\circ)^c) \leq \delta_{k(n)} + \Pr(\mathcal{E}_n^\circ(\rho)^c) \longrightarrow 0, \tag{C.17}$$

with $\Omega_n^\circ = \varnothing$ for $n < n_1$.

On Ω_n° the length error is less than $\delta_{k(n)}$. Continuity of Ψ_s° from Theorem B.3, the gradient CLT, and Slutsky's theorem prove (6.5). For existence, put $B_s^\circ = \{g : 0 < |g| < t_{\mathrm{circ}}(s)\}$ if $s > 0$ and $B_s^\circ = \varnothing$ otherwise. The indicator identity gives the separate bound

$$|\Pr(L_n^\circ > 0) - \Pr(G_n^\circ \in B_s^\circ)| \leq \Pr((\Omega_n^\circ)^c) \longrightarrow 0.$$

The limiting Gaussian gives zero mass to the origin and threshold circle; its Rayleigh radial law proves (6.6), including the zero limit when $s \leq 0$. These events also establish the complete-module assertion of Theorem 6.1.

C.6 Examples and the fourth-moment condition

For a regular k-gon, averaging $e^{ij\phi}$ gives zero unless k divides j. Restrictions of degree-four polynomials to the circle use only Fourier orders at most four, so (6.1) holds exactly for $k \geq 5$. Even k supplies central symmetry, preserved by arbitrary mixtures of rotations. The density

$$\frac{1 + \alpha\cos(6\phi) + \beta\cos(10\phi)}{2\pi}, \qquad |\alpha| + |\beta| < 1,$$

also satisfies the assumptions. When both coefficients are nonzero its rotation group is exactly C_2; the density is analytic and also reflection symmetric.

For the uniform square, $\mathbb{E}U^4$ is $1/2$ on an axis and $1/4$ on a diagonal. Its critical quartic coefficient divided by C_{circ} is $[-1/8 + \mathbb{E}U^4/6]/v^2$, hence respectively $-1/(24v^2)$ and $-1/(12v^2)$. Thus second-moment isotropy alone does not determine an isotropic fourth-order expansion; this comparison does not identify the square's persistence law. Odd regular $k \geq 5$ match the fourth-order expansion and gradient covariance but lack central symmetry. The exterior argument (C.9) proves the stated centrally symmetric case. Higher-order corrections and uniformity over angular laws are separate extensions.

Supplementary information

Online Resource 1 contains additional results on boundary and critical-height localization, translation and angular-average centers, and a single added kernel. It uses the model and notation of this article; the main theorem does not rely on these additional results.

Statements and declarations

Funding

The author received no specific funding for this work.

Competing interests

The author declares no competing interests.

Data and code availability

The numerical studies use synthetic samples. The simulation code, fixed experimental designs, saved numerical results, and associated error-budget records are available at https://github.com/Jiaxuanren030125/planar-kde-persistence-code.

References

Bobrowski, O., Mukherjee, S., Taylor, J.E.: Topological consistency via kernel estimation. Bernoulli **23**(1), 288–328 (2017) https://doi.org/10.3150/15-BEJ744

Carlsson, E., Carlsson, J.: Alpha shapes in kernel density estimation. Journal of Applied and Computational Topology **10** (2026) https://doi.org/10.1007/s41468-026-00241-3 . Article 18

Chazal, F., Fasy, B., Lecci, F., Michel, B., Rinaldo, A., Wasserman, L.: Robust topological inference: Distance to a measure and kernel distance. Journal of Machine Learning Research **18**(159), 1–40 (2018). Published article: https://www.jmlr.org/papers/volume18/15-484/15-484.pdf

Chen, Q., Fang, Z.: Inference on functionals under first order degeneracy. Journal of Econometrics **210**(2), 459–481 (2019) https://doi.org/10.1016/j.jeconom.2019.01.011 . Preprint version: arXiv:1901.04861v1

Cohen-Steiner, D., Edelsbrunner, H., Harer, J.: Stability of persistence diagrams. Discrete & Computational Geometry **37**(1), 103–120 (2007) https://doi.org/10.1007/s00454-006-1276-5

Coste, M.: An Introduction to O-minimal Geometry. Institut de Recherche Mathématique de Rennes, Rennes (1999). Lecture notes: https://perso.univ-rennes1.fr/michel.coste/polyens/OMIN.pdf

Eltzner, B., Huckemann, S.F.: A smeary central limit theorem for manifolds with application to high-dimensional spheres. The Annals of Statistics **47**(6), 3360–3381 (2019) https://doi.org/10.1214/18-AOS1781 . Preprint version: arXiv:1801.06581v1

Fasy, B.T., Lecci, F., Rinaldo, A., Wasserman, L., Balakrishnan, S., Singh, A.: Confidence sets for persistence diagrams. The Annals of Statistics **42**(6), 2301–2339 (2014) https://doi.org/10.1214/14-AOS1252

Hall, P., Ooi, H.: Attributing a probability to the shape of a probability density. The Annals of Statistics **32**(5), 2098–2123 (2004). Electronic reprint: https://arxiv.org/pdf/math/0503675v1

Hatcher, A.: Algebraic Topology. Cambridge University Press, Cambridge (2002)

Milnor, J.: Morse Theory. Annals of Mathematics Studies, vol. 51. Princeton University Press, Princeton, NJ (1963)

Phillips, J.M., Wang, B., Zheng, Y.: Geometric inference on kernel density estimates. In: 31st International Symposium on Computational Geometry. LIPIcs, vol. 34, pp. 857–871 (2015). https://doi.org/10.4230/LIPIcs.SOCG.2015.857

Pike, J.A., Khan, A.O., Pallini, C., Thomas, S.G., Mund, M., Ries, J., Poulter, N.S., Styles, I.B.: Topological data analysis quantifies biological nano-structure from single molecule localization microscopy. Bioinformatics **36**(5), 1614–1621 (2020) https://doi.org/10.1093/bioinformatics/btz788

Thomas, A.M.: Convergence of persistence diagrams for discrete time stationary processes. Journal of Applied and Computational Topology **9** (2025) https://doi.org/10.1007/s41468-025-00211-1 . Article 14

Tran, D.: Behavior of the Fréchet mean and central limit theorems on spheres. Brazilian Journal of Probability and Statistics **35**(3), 590–608 (2021) https://doi.org/10.1214/21-BJPS499 . Preprint version: arXiv:1911.01985v2

van den Dries, L., Miller, C.: Geometric categories and o-minimal structures. Duke Mathematical Journal **84**(2), 497–540 (1996). Author revision, 20 February 2001: https://people.math.osu.edu/miller.1987/newg.pdf; section references are to this revision

Yu, Y.: The Shape of the Noncentral Chi-square Density. arXiv:1106.5241 (2011). https://arxiv.org/abs/1106.5241

Supplementary Files

This is a list of supplementary files associated with this preprint. Click to download.

- ESM1.pdf